Robust a posteriori error estimation for stochastic Galerkin formulations of parameter dependent linear elasticity equations

Khan, Arbaz; Bespalov, Alex; Powell, Catherine; Silvester, David

DOI:
10.1090/mcom/3572

ROBUST A POSTERIORI ERROR ESTIMATION FOR PARAMETER-DEPENDENT LINEAR ELASTICITY EQUATIONS

ARBAZ KHAN, ALEX BESPALOV, CATHERINE E. POWELL, AND DAVID J. SILVESTER

Abstract. The focus of this work is a posteriori error estimation for stochastic Galerkin approximations of parameter-dependent linear elasticity equations. The starting point is a three-field partial differential equation model with the Young modulus represented as an affine function of a countable set of parameters. We introduce a weak formulation, establish its stability with respect to a weighted norm and discuss its approximation using stochastic Galerkin mixed finite element methods. We motivate an a posteriori error estimation scheme and establish upper and lower bounds for the approximation error. The constants in the bounds are independent of the Poisson ratio as well as the spatial and parametric discretisation parameters. We also discuss proxies for the error reduction associated with enrichments of the approximation spaces and we develop an adaptive algorithm that terminates when the estimated error falls below a user-prescribed tolerance. The error reduction proxies are shown to be reliable and efficient in the incompressible limit case. Numerical results are presented to supplement the theory. All experiments were performed using open source (IFISS) software that is available online.

1. Introduction

The motivation for this work is the need to develop accurate and efficient numerical algorithms for solving linear elasticity problems in engineering applications where Young's modulus is spatially varying in an uncertain way. Of particular interest is the nearly incompressible case, which poses a significant challenge for numerical methods, even when all the model inputs are known exactly. An established strategy for avoiding locking of finite element methods for standard elasticity problems is to introduce an auxiliary pressure variable, obtain a coupled system of partial differential equations (PDEs) and then to apply mixed finite element methods; see, for example, [18, 8, 21]. Error estimates for the resulting locking-free formulation can be found in Houston et al. [20] and Kouhia & Stenberg [23]. Recently, in [22], Khan et al. introduced a three-field PDE model with a parameter-dependent Young's modulus which is amenable to discretisation by stochastic Galerkin mixed finite element methods (SG-MFEMs). The focus in [22] is on efficient linear algebra—error estimation is not considered. The three-field model

Date: June 24, 2020.

1991 *Mathematics Subject Classification.* 65N30, 65N15, 35R60.

Key words and phrases. uncertainty quantification, linear elasticity, mixed approximation, stochastic Galerkin finite element method, a posteriori error estimation, adaptivity.

This work was supported by EPSRC grants EP/P013317/1 and EP/P013791/1. The authors would also like to thank the Isaac Newton Institute for Mathematical Sciences, Cambridge, for support and hospitality during the Uncertainty Quantification programme which was supported by EPSRC grant EP/K032208/1.

The third author acknowledges the support of the Simons Foundation.

is analysed in detail in this paper. Specifically we introduce an effective a posteriori error estimation strategy that is robust in the incompressible limit case. The novel aspect of this work is the construction of an adaptive refinement algorithm that automatically balances the spatial discretisation error with the parametric discretisation error. The adaptivity is driven by error reduction proxies that have a rigorous underpinning.

While there has been little work to date on a posteriori error estimation and adaptivity for stochastic Galerkin approximations of *mixed* formulations of linear elasticity problems, the primal problem has been extensively studied in the literature. Specifically, stochastic finite element methods are discussed in [16, 27] and the references therein. In [24], Matthies et al. provide an overview of how to incorporate uncertainty into material parameters in linear elasticity problems. A framework for residual-based a posteriori error estimation and adaptive stochastic Galerkin approximation for second order linear elliptic PDEs is presented in [12]. Numerical results are presented for planar linear elasticity problems but the incompressible limit is not considered. The theoretical basis for automatic refinement algorithms for parametric PDE problems has been established in the last decade. Building on the pioneering work of Cohen et al., see [9], recent work by Bachmayr et al. [2] and by Crowder et al. [11] opens up the possibility of designing optimal algorithms from a best approximation perspective. A priori analysis for so-called best N-term approximations of standard mixed formulations of stochastic and multiscale elasticity problems can be found in [30, 19]. Error estimation and adaptivity in a sparse grid collocation context is discussed in [17].

The formal mathematical specification of the problem we consider is as follows. Let D (the spatial domain) be a bounded Lipschitz polygon in $\mathbb{R}^2$ (polyhedron in $\mathbb{R}^3$) with boundary $\partial D = \partial D_D \cup \partial D_N$, where $\partial D_D \cap \partial D_N = \emptyset$ and $\partial D_D, \partial D_N \neq \emptyset$.[1] Next, we introduce a vector of countably many parameters $\boldsymbol{y} = (y_1, y_2, \ldots)$ with each $y_k \in \Gamma_k := [-1, 1]$. We model Young's modulus in the linear elasticity equations as a parameter-dependent function of the form

$$E(\boldsymbol{x}, \boldsymbol{y}) := e_0(\boldsymbol{x}) + \sum_{k=1}^{\infty} e_k(\boldsymbol{x}) y_k, \quad \boldsymbol{x} \in D, \quad \boldsymbol{y} \in \Gamma. \tag{1}$$

In (1), $\Gamma := \Pi_{k=1}^{\infty} \Gamma_k$ denotes the parameter domain and e_0 typically represents the mean of E. The parameters y_k are images of mean zero random variables and these encode our uncertainty about E. Picking a specific $\mathbf{y} \in \Gamma$ corresponds to generating a realisation of E. Following [22], we consider the (*three-field*) parametric problem: find $\boldsymbol{u} : D \times \Gamma \to \mathbb{R}^d$ $(d = 2, 3)$ and $p, \tilde{p} : D \times \Gamma \to \mathbb{R}$ such that

$$-\nabla \cdot \boldsymbol{\sigma}(\boldsymbol{x}, \boldsymbol{y}) = \boldsymbol{f}(\boldsymbol{x}), \quad \boldsymbol{x} \in D, \ \boldsymbol{y} \in \Gamma, \tag{2a}$$

$$\nabla \cdot \boldsymbol{u}(\boldsymbol{x}, \boldsymbol{y}) + \tilde{\lambda}^{-1} \tilde{p}(\boldsymbol{x}, \boldsymbol{y}) = 0, \quad \boldsymbol{x} \in D, \ \boldsymbol{y} \in \Gamma, \tag{2b}$$

$$\tilde{\lambda}^{-1} p(\boldsymbol{x}, \boldsymbol{y}) - \tilde{\lambda}^{-1} E(\boldsymbol{x}, \boldsymbol{y}) \tilde{p}(\boldsymbol{x}, \boldsymbol{y}) = 0, \quad \boldsymbol{x} \in D, \ \boldsymbol{y} \in \Gamma, \tag{2c}$$

$$\boldsymbol{u}(\boldsymbol{x}, \boldsymbol{y}) = \boldsymbol{g}(\boldsymbol{x}), \quad \boldsymbol{x} \in \partial D_D, \ \boldsymbol{y} \in \Gamma, \tag{2d}$$

$$\boldsymbol{\sigma}(\boldsymbol{x}, \boldsymbol{y})\, \boldsymbol{n} = \mathbf{0}, \quad \boldsymbol{x} \in \partial D_N, \ \boldsymbol{y} \in \Gamma. \tag{2e}$$

[1] Our analysis can be extended to cover the Dirichlet case $\partial D = \partial D_D$ by redefining the approximation spaces to ensure uniqueness of pressure in the incompressible limit.

Here, $\boldsymbol{\sigma} : D \times \Gamma \to \mathbb{R}^{d\times d}$ is the stress tensor, $\boldsymbol{f} : D \to \mathbb{R}^d$ is the body force, $\boldsymbol{n}$ denotes the outward unit normal vector to ∂D_N, $\boldsymbol{u}$ is the displacement (the solution field of main interest) and the auxiliary variables that we have introduced are $p := -\lambda \nabla \cdot \boldsymbol{u}$ (the so-called Herrmann pressure [18]) and $\tilde{p} := p/E$. Recall that $\boldsymbol{\sigma}$ is related to the strain tensor $\boldsymbol{\varepsilon} : D \times \Gamma \to \mathbb{R}^{d\times d}$ through the identities $\boldsymbol{\sigma} = 2\mu\boldsymbol{\varepsilon} - p\boldsymbol{I}$ and $\boldsymbol{\varepsilon} = \frac{1}{2}\left(\nabla \boldsymbol{u} + (\nabla \boldsymbol{u})^\top\right)$. The Lamé coefficients are

$$\mu(\boldsymbol{x},\boldsymbol{y}) = \frac{E(\boldsymbol{x},\boldsymbol{y})}{2(1+\nu)}, \quad \lambda(\boldsymbol{x},\boldsymbol{y}) = \frac{E(\boldsymbol{x},\boldsymbol{y})\nu}{(1+\nu)(1-2\nu)}$$

and we have also introduced the constant

$$\tilde{\lambda} := \frac{\lambda(\boldsymbol{x},\boldsymbol{y})}{E(\boldsymbol{x},\boldsymbol{y})} = \frac{\nu}{(1+\nu)(1-2\nu)}.$$

We assume that the Poisson ratio $\nu \in (0, 1/2)$ is a given fixed constant (and hence, so is $\tilde{\lambda}$) and that $0 < \mu_1 < \mu < \mu_2 < \infty$ and $0 < \lambda < \infty$ a.e. in $D \times \Gamma$. In contrast to other mixed formulations of the linear elasticity equations, the advantage of (2) is that while E appears in the first and third equations, E^{-1} does not appear at all. As a result, since E has the affine form (1), the discrete problem associated with SG-MFEM approximations has a structure that is relatively easy to exploit.

In Section 2 we recall the weak formulation of (2) and discuss stability and well-posedness. A key feature of our analysis is that we work with a ν-dependent norm. In Section 3, we discuss SG-MFEM approximation and set up the associated finite-dimensional weak problem. In Section 4 we extend the standard hierarchical a posteriori error estimation strategy of Bank & Smith [3] to accommodate the parametric components of the approximation. We then establish two-sided bounds for the true error in terms of the proposed estimate. The constants in the bounds are independent of the Poisson ratio, so that the error estimation is robust in the incompressible limit $\nu \to 1/2$. In Section 5 we introduce proxies for the error reductions that would be achieved by performing finite element mesh refinement, or by enriching the parametric part of the approximation space. We establish two-sided bounds, showing that these error reduction proxies are efficient and reliable. The proxies are incorporated within an adaptive refinement procedure in Section 6 and the effectiveness of the adaptive algorithm is demonstrated computationally by the numerical results reported in Section 7.

2. Weak formulation

Before stating the weak formulation of (2), we recall the conditions on the Young modulus E that are required to establish well-posedness and define appropriate solution spaces. Note that E takes the specific form (1) with $y_k \in [-1, 1]$.

Assumption 2.1. *The random field E is an essentially bounded measurable function $E \in L^\infty(D\times\Gamma)$ that is uniformly bounded away from zero. That is, there exist positive constants $E_{\min}$ and $E_{\max}$ such that*

$$0 < E_{\min} \le E(\boldsymbol{x},\boldsymbol{y}) \le E_{\max} < \infty \quad \text{a.e. in } D\times\Gamma. \tag{3}$$

The lower bound in (3) *is satisfied by making the further assumption that*

$$0 < e_0^{\min} \le e_0(\boldsymbol{x}) \le e_0^{\max} < \infty \ \ \textit{a.e. in } D \quad \textit{and} \quad \frac{1}{e_0^{\min}} \sum_{k=1}^{\infty} \|e_k\|_{L^\infty(D)} < 1. \tag{4}$$

Let $\pi(\boldsymbol{y})$ be a product measure with $\pi(\boldsymbol{y}) := \Pi_{k=1}^{\infty}\pi_k(y_k)$, where π_k is a measure on $(\Gamma_k, \mathcal{B}(\Gamma_k))$ and $\mathcal{B}(\Gamma_k)$ is the Borel σ-algebra on $\Gamma_k = [-1, 1]$. We will assume that the parameters y_k in (1) are images of independent uniform random variables $\xi_k \sim U(-1, 1)$ and choose π_k to be the associated probability measure. In this case, π_k has density $\rho_k = 1/2$ with respect to Lebesgue measure and

$$\int_{\Gamma_k} y_k \, d\pi_k(y_k) = \int_{\Gamma_k} y_k(1/2)dy_k = 0.$$

Now, given a normed linear space $X(D)$ of real-valued functions on D (either vector or scalar valued) with norm $\|\cdot\|_X$, we can define the Bochner space (for example, in the case of vector-valued functions) as follows:

$$L^2_\pi(\Gamma, X(D)) := \left\{\boldsymbol{v}(\boldsymbol{x}, \boldsymbol{y}) : D \times \Gamma \to \mathbb{R}^d; \|\boldsymbol{v}\|_{L^2_\pi(\Gamma, X(D))} < \infty\right\},$$

where

$$\|\cdot\|_{L^2_\pi(\Gamma, X(D))} := \left(\int_\Gamma \|\cdot\|^2_X d\pi(\boldsymbol{y})\right)^{1/2}. \tag{5}$$

In particular, we will need the spaces

$$\boldsymbol{\mathcal{V}} := L^2_\pi(\Gamma, \boldsymbol{H}^1_{E_0}(D)), \quad \mathcal{W} := L^2_\pi(\Gamma, L^2(D)) \quad \text{and} \quad \boldsymbol{\mathcal{W}} := L^2_\pi(\Gamma, \boldsymbol{L}^2(D)), \tag{6}$$

where $\boldsymbol{H}^1_{E_0}(D) := \{\boldsymbol{v} \in \boldsymbol{H}^1(D), \boldsymbol{v}|_{\partial D_D} = \boldsymbol{0}\}$ and $\boldsymbol{H}^1(D)$, $\boldsymbol{L}^2(D)$ are the usual vector-valued Sobolev spaces. We denote the norms (5) associated with $\boldsymbol{\mathcal{V}}$, $\mathcal{W}$ and $\boldsymbol{\mathcal{W}}$ by $\|\cdot\|_{\boldsymbol{\mathcal{V}}}$, $\|\cdot\|_{\mathcal{W}}$ and $\|\cdot\|_{\boldsymbol{\mathcal{W}}}$, respectively.

Assume that the load function $\boldsymbol{f} \in \boldsymbol{L}^2(D)$ and the boundary data $\boldsymbol{g} = \boldsymbol{0}$ on ∂D_D. Then, the weak formulation of (2) is: find $(\boldsymbol{u}, p, \tilde{p}) \in \boldsymbol{\mathcal{V}} \times \mathcal{W} \times \mathcal{W}$ such that

$$a(\boldsymbol{u}, \boldsymbol{v}) + b(\boldsymbol{v}, p) = f(\boldsymbol{v}) \quad \forall \boldsymbol{v} \in \boldsymbol{\mathcal{V}}, \tag{7a}$$

$$b(\boldsymbol{u}, q) - c(\tilde{p}, q) = 0 \qquad \forall q \in \mathcal{W}, \tag{7b}$$

$$-c(p, \tilde{q}) + d(\tilde{p}, \tilde{q}) = 0 \qquad \forall \tilde{q} \in \mathcal{W}, \tag{7c}$$

where we have

$$a(\boldsymbol{u}, \boldsymbol{v}) := \alpha \int_\Gamma \int_D E(\boldsymbol{x}, \boldsymbol{y})\boldsymbol{\varepsilon}(\boldsymbol{u}(\boldsymbol{x}, \boldsymbol{y})) : \boldsymbol{\varepsilon}(\boldsymbol{v}(\boldsymbol{x}, \boldsymbol{y}))d\boldsymbol{x}d\pi(\boldsymbol{y}), \tag{8}$$

$$b(\boldsymbol{v}, p) := -\int_\Gamma \int_D p(\boldsymbol{x}, \boldsymbol{y})\nabla \cdot \boldsymbol{v}(\boldsymbol{x}, \boldsymbol{y})d\boldsymbol{x}d\pi(\boldsymbol{y}), \tag{9}$$

$$c(p, q) := (\alpha\beta)^{-1} \int_\Gamma \int_D p(\boldsymbol{x}, \boldsymbol{y})q(\boldsymbol{x}, \boldsymbol{y})d\boldsymbol{x}d\pi(\boldsymbol{y}), \tag{10}$$

$$d(p, q) := (\alpha\beta)^{-1} \int_\Gamma \int_D E(\boldsymbol{x}, \boldsymbol{y})p(\boldsymbol{x}, \boldsymbol{y})q(\boldsymbol{x}, \boldsymbol{y})d\boldsymbol{x}d\pi(\boldsymbol{y}), \tag{11}$$

$$f(\boldsymbol{v}) := \int_\Gamma \int_D f(\boldsymbol{x})\boldsymbol{v}(\boldsymbol{x}, \boldsymbol{y})d\boldsymbol{x}d\pi(\boldsymbol{y}), \tag{12}$$

and we define the constants

$$\alpha := \frac{1}{1+\nu}, \qquad \beta := \frac{\nu}{(1-2\nu)}. \tag{13}$$

Note that $\alpha\beta = \tilde{\lambda}$. Furthermore, it is important to note that the constants α and β depend only on the Poisson ratio ν which is assumed to be known. It will also be useful to define the combined bilinear form

$$\mathcal{B}(\boldsymbol{u}, p, \tilde{p}; \boldsymbol{v}, q, \tilde{q}) = a(\boldsymbol{u}, \boldsymbol{v}) + b(\boldsymbol{v}, p) + b(\boldsymbol{u}, q) - c(\tilde{p}, q) - c(p, \tilde{q}) + d(\tilde{p}, \tilde{q}), \tag{14}$$

so as to express (7) more compactly as: find $(\boldsymbol{u}, p, \tilde{p}) \in \boldsymbol{\mathcal{V}} \times \mathcal{W} \times \mathcal{W}$ such that

$$\mathcal{B}(\boldsymbol{u}, p, \tilde{p}; \boldsymbol{v}, q, \tilde{q}) = f(\boldsymbol{v}) \quad \forall (\boldsymbol{v}, q, \tilde{q}) \in \boldsymbol{\mathcal{V}} \times \mathcal{W} \times \mathcal{W}. \tag{15}$$

In the limit $\nu \to 1/2$, observe that $\beta \to \infty$ and so $c(\cdot,\cdot)$ and $d(\cdot,\cdot)$ disappear from (7) and (15), yielding a standard Stokes-like system. See Section 6 for more details.

To analyse the error associated with a stochastic Galerkin approximation of the weak solution, we will work with the ν-dependent norm $|||\cdot|||$ on $\boldsymbol{\mathcal{V}} \times \mathcal{W} \times \mathcal{W}$ introduced in [22] and defined by

$$|||(\boldsymbol{v}, q, \tilde{q})|||^2 := \alpha \|\nabla \boldsymbol{v}\|^2_{\boldsymbol{\mathcal{W}}} + (\alpha^{-1} + (\alpha\beta)^{-1}) \|q\|^2_{\mathcal{W}} + (\alpha\beta)^{-1} \|\tilde{q}\|^2_{\mathcal{W}}. \tag{16}$$

The motivation for this specific choice of norm is the following stability result.

Lemma 2.1. [22, Lemma 2.3] *If Assumption 2.1 holds, then for any $(\boldsymbol{u}, p, \tilde{p}) \in \boldsymbol{\mathcal{V}} \times \mathcal{W} \times \mathcal{W}$, there exists a function triple $(\boldsymbol{v}, q, \tilde{q}) \in \boldsymbol{\mathcal{V}} \times \mathcal{W} \times \mathcal{W}$ with $|||(\boldsymbol{v}, q, \tilde{q})||| \leq C_2 \, |||(\boldsymbol{u}, p, \tilde{p})|||$, satisfying*

$$\mathcal{B}(\boldsymbol{u}, p, \tilde{p}; \boldsymbol{v}, q, \tilde{q}) \geq E_{\min} \, C_1 \, |||(\boldsymbol{u}, p, \tilde{p})|||^2, \tag{17}$$

with constants $C_1 = \frac{1}{2} \min\{C_K, \frac{C_D^2}{E_{\max}^2}, \frac{1}{E_{max}^2}\}$ and $C_2 = \sqrt{2(E_{\max}^2 + C_D^2 + 1)}/E_{\max}$, where C_K is the Korn constant and $E_{\min}$, $E_{\max}$ are the upper and lower bounds for the Young modulus. The inf–sup constant $C_D > 0$ depends only on D and is given by

$$\sup_{0 \neq \boldsymbol{v} \in \boldsymbol{\mathcal{V}}} \frac{b(\boldsymbol{v}, q)}{\|\nabla \boldsymbol{v}\|_{\boldsymbol{\mathcal{W}}}} \geq C_D \|q\|_{\mathcal{W}} \quad \forall q \in \mathcal{W}. \tag{18}$$

The well-posedness of (15) is thus guaranteed; see [22, Theorem 2.4].

3. Stochastic Galerkin mixed finite element approximation

To approximate solutions to (7), or equivalently (15), we begin by choosing finite-dimensional subspaces of $\boldsymbol{\mathcal{V}}$ and $\mathcal{W}$. Our construction exploits the fact that $\boldsymbol{\mathcal{V}} \cong \boldsymbol{H}^1_{E_0}(D) \otimes L^2_\pi(\Gamma)$ and $\mathcal{W} \cong L^2(D) \otimes L^2_\pi(\Gamma)$ (i.e., that the spaces are isometrically isomorphic). First, we introduce a mesh $\mathcal{T}_h$ on the physical domain D with characteristic mesh size h and choose a pair of conforming finite element spaces

$$V_h := \text{span}\,\{\phi_r(\boldsymbol{x})\}_{r=1}^{n_u} \subset H^1_{E_0}(D), \qquad W_h := \text{span}\,\{\varphi_s(\boldsymbol{x})\}_{s=1}^{n_p} \subset L^2(D).$$

We then define $\boldsymbol{V}_h$ to be the space of vector-valued functions whose components are in V_h. We need $\boldsymbol{V}_h$ and W_h to be compatible in the sense that they satisfy the *discrete* (deterministic) inf–sup condition

$$\sup_{0 \neq \boldsymbol{v} \in \boldsymbol{V}_h} \frac{\int_D q \, \nabla \cdot \boldsymbol{v}}{\|\nabla \boldsymbol{v}\|_{\boldsymbol{L}^2(D)}} \geq \gamma_h \|q\|_{L^2(D)} \quad \forall q \in W_h, \tag{19}$$

with γ_h uniformly bounded away from zero (i.e., independent of h). Stable mixed approximation pairs satisfying (19) are known as *Stokes elements*. Two popular examples of stable rectangular element approximations are $\boldsymbol{Q}_2$–Q_1 (continuous biquadratic approximation for the displacement and continuous bilinear approximation for the pressure) and $\boldsymbol{Q}_2$–P_{-1} (continuous biquadratic approximation for the displacement and discontinuous linear approximation for the pressure). Both approximation strategies are inf–sup stable in a two and three-dimensional setting.

Next, we consider the parametric discretisation. Let $\{\psi_i(y_j), i = 0, 1, \ldots\}$ denote the set of univariate Legendre polynomials on $\Gamma_j = [-1, 1]$, where $j \in \mathbb{N}$ and ψ_i has

degree i. We fix $\psi_0 = 1$ and assume that the polynomials are normalised so that $\int_{\Gamma_j} \psi_i(y_j)\psi_k(y_j)d\pi_j(y_j) = \delta_{i,k}$. We define the set of finitely supported sequences $\mathfrak{J} := \{\boldsymbol{\alpha} = (\alpha_1, \alpha_2, \ldots) \in \mathbb{N}_0^{\mathbb{N}};\ \#\operatorname{supp}\boldsymbol{\alpha} < \infty\}$, where $\operatorname{supp}\boldsymbol{\alpha} := \{m \in \mathbb{N};\ \alpha_m \neq 0\}$. The set $\mathfrak{J}$ and its subsets will be called 'index sets'. Combining these ingredients, we then define the countable set of multivariate tensor product polynomials

$$\psi_{\boldsymbol{\alpha}}(\boldsymbol{y}) := \prod_{i=1}^{\infty} \psi_{\alpha_i}(y_i) \quad \forall \boldsymbol{\alpha} \in \mathfrak{J} \tag{20}$$

which forms an orthonormal basis for $L^2_\pi(\Gamma)$. Now, given any finite index set $\Lambda \subset \mathfrak{J}$, we can define a finite-dimensional subspace of $L^2_\pi(\Gamma)$ as follows:

$$S_\Lambda := \operatorname{span}\{\psi_{\boldsymbol{\alpha}};\ \ \boldsymbol{\alpha} \in \Lambda\}. \tag{21}$$

Note that only a *finite* number of parameters y_k play a role in the definition of S_Λ.

Finally, we define the SG-MFEM approximation spaces

$$\boldsymbol{V}_{h,\Lambda} := \boldsymbol{V}_h \otimes S_\Lambda, \qquad W_{h,\Lambda} := W_h \otimes S_\Lambda,$$

and consider the problem: find $(\boldsymbol{u}_{h,\Lambda}, p_{h,\Lambda}, \tilde{p}_{h,\Lambda}) \in \boldsymbol{V}_{h,\Lambda} \times W_{h,\Lambda} \times W_{h,\Lambda}$ such that

$$a(\boldsymbol{u}_{h,\Lambda}, \boldsymbol{v}) + b(\boldsymbol{v}, p_{h,\Lambda}) = f(\boldsymbol{v}) \quad \forall \boldsymbol{v} \in \boldsymbol{V}_{h,\Lambda}, \tag{22a}$$

$$b(\boldsymbol{u}_{h,\Lambda}, q) - c(\tilde{p}_{h,\Lambda}, q) = 0 \qquad \forall q \in W_{h,\Lambda}, \tag{22b}$$

$$-c(p_{h,\Lambda}, \tilde{q}) + d(\tilde{p}_{h,\Lambda}, \tilde{q}) = 0 \qquad \forall \tilde{q} \in W_{h,\Lambda}. \tag{22c}$$

The well-posedness of (22) is established using the following discrete stability result.

Lemma 3.1. *If E satisfies Assumption 2.1, and $\boldsymbol{V}_h, W_h$ satisfy the inf–sup condition* (19) *with $\gamma_h > 0$, then for every $(\boldsymbol{u}_{h,\Lambda}, p_{h,\Lambda}, \tilde{p}_{h,\Lambda}) \in \boldsymbol{V}_{h,\Lambda} \times W_{h,\Lambda} \times W_{h,\Lambda}$, there exists $(\boldsymbol{v}, q, \tilde{q}) \in \boldsymbol{V}_{h,\Lambda} \times W_{h,\Lambda} \times W_{h,\Lambda}$ with $|||(\boldsymbol{v}, q, \tilde{q})||| \leq C_2^* \, |||(\boldsymbol{u}_{h,\Lambda}, p_{h,\Lambda}, \tilde{p}_{h,\Lambda})|||$, satisfying*

$$\mathcal{B}(\boldsymbol{u}_{h,\Lambda}, p_{h,\Lambda}, \tilde{p}_{h,\Lambda}; \boldsymbol{v}, q, \tilde{q}) \geq E_{\min}\, C_1^* \, |||(\boldsymbol{u}_{h,\Lambda}, p_{h,\Lambda}, \tilde{p}_{h,\Lambda})|||^2, \tag{23}$$

where $C_1^* := \frac{1}{2}\min\{C_K, \frac{\gamma_h^2}{E_{\max}^2}, \frac{1}{E_{\max}^2}\}$, $C_2^* := \sqrt{2(E_{\max}^2 + \gamma_h^2 + 1)}/E_{\max}$ and C_K is the Korn constant.

Proof. The proof follows the same lines as that of Lemma 2.1, which is given in [22, Lemma 2.3]. Note that the constants C_1^* and C_2^* depend on the *discrete* inf–sup constant γ_h that is associated with the specific choice of finite element spaces $\boldsymbol{V}_h$ and W_h. □

In the next section, we will outline and analyse a strategy for estimating the SG-MFEM errors $\boldsymbol{e}^{\boldsymbol{u}} := \boldsymbol{u} - \boldsymbol{u}_{h,\Lambda}$, $e^p := p - p_{h,\Lambda}$ and $e^{\tilde{p}} := \tilde{p} - \tilde{p}_{h,\Lambda}$. To do this, we will follow the construction of Bank & Smith [3], and introduce hierarchical spaces that are richer than the chosen $\boldsymbol{V}_{h,\Lambda}$ and $W_{h,\Lambda}$. Specifically, we let $\boldsymbol{V}_h^*$ and W_h^* be an inf–sup stable pair of conforming mixed finite element spaces with $\boldsymbol{V}_h \subset \boldsymbol{V}_h^*$ and $W_h \subset W_h^*$ such that

$$\boldsymbol{V}_h^* = \boldsymbol{V}_h \oplus \widetilde{\boldsymbol{V}}_h \quad \text{and} \quad W_h^* = W_h \oplus \widetilde{W}_h, \tag{24}$$

where $\widetilde{\boldsymbol{V}}_h \subset \boldsymbol{H}^1_{E_0}(D)$, $\widetilde{W}_h \subset L^2(D)$, and

$$\boldsymbol{V}_h \cap \widetilde{\boldsymbol{V}}_h = \{\boldsymbol{0}\}, \qquad W_h \cap \widetilde{W}_h = \{0\}. \tag{25}$$

We will refer to $\widetilde{\boldsymbol{V}}_h$ and $\widetilde{W}_h$ as the finite element *detail spaces*. For example, these could be constructed from basis functions that would be introduced by performing a uniform refinement of the mesh associated with $\boldsymbol{V}_h$ and W_h. Since $\boldsymbol{H}^1_{E_0}(D)$ and $L^2(D)$ are Hilbert spaces and (25) holds, then, by the strengthened Cauchy–Schwarz inequality [1, 13, 10], there exist constants $\gamma_1, \gamma_2 \in [0,1)$ (known as CBS constants) such that

$$\left| \int_D \nabla \boldsymbol{v} : \nabla \widetilde{\boldsymbol{v}} \right| \leq \gamma_1 \, \|\nabla \boldsymbol{v}\|_{\boldsymbol{L}^2(D)} \|\nabla \widetilde{\boldsymbol{v}}\|_{\boldsymbol{L}^2(D)} \quad \forall \boldsymbol{v} \in \boldsymbol{V}_h, \, \forall \widetilde{\boldsymbol{v}} \in \widetilde{\boldsymbol{V}}_h, \tag{26a}$$

$$\left| \int_D q \, \widetilde{q} \right| \leq \gamma_2 \, \|q\|_{L^2(D)} \, \|\tilde{q}\|_{L^2(D)} \qquad \forall q \in W_h, \, \forall \widetilde{q} \in \widetilde{W}_h. \tag{26b}$$

Next, suppose we choose a new index set $\mathfrak{Q} \subset \mathfrak{I}$ such that $\Lambda \cap \mathfrak{Q} = \emptyset$ and define $\Lambda^* := \Lambda \cup \mathfrak{Q}$. We will refer to $\mathfrak{Q}$ as the *detail index set*. On the parameter domain Γ, we can then define an enriched polynomial space $S^*_\Lambda := \operatorname{span}\{\psi_{\boldsymbol{\alpha}}; \ \boldsymbol{\alpha} \in \Lambda^*\} \subset L^2_\pi(\Gamma)$. Moreover, we have

$$S^*_\Lambda = S_\Lambda \oplus S_\mathfrak{Q}, \quad S_\Lambda \cap S_\mathfrak{Q} = \{0\}. \tag{27}$$

We can now construct enriched finite-dimensional subspaces of $\boldsymbol{\mathcal{V}}$ and $\mathcal{W}$ using the finite element detail spaces $\widetilde{\boldsymbol{V}}_h$, $\widetilde{W}_h$ and the polynomial space $S_\mathfrak{Q}$,

$$\boldsymbol{V}^*_{h,\Lambda} := \boldsymbol{V}_{h^*,\Lambda} \oplus \boldsymbol{V}_{h,\mathfrak{Q}} = \boldsymbol{V}_{h,\Lambda} \oplus \widetilde{\boldsymbol{V}}_{h,\Lambda} \oplus \boldsymbol{V}_{h,\mathfrak{Q}} = \boldsymbol{V}_{h,\Lambda} \oplus \Big(\widetilde{\boldsymbol{V}}_{h,\Lambda} \oplus \boldsymbol{V}_{h,\mathfrak{Q}} \Big), \tag{28}$$

$$W^*_{h,\Lambda} := W_{h^*,\Lambda} \oplus W_{h,\mathfrak{Q}} = W_{h,\Lambda} \oplus \widetilde{W}_{h,\Lambda} \oplus W_{h,\mathfrak{Q}} = W_{h,\Lambda} \oplus \Big(\widetilde{W}_{h,\Lambda} \oplus W_{h,\mathfrak{Q}} \Big), \tag{29}$$

where $\boldsymbol{V}_{h^*,\Lambda} := \boldsymbol{V}^*_h \otimes S_\Lambda$, $W_{h^*,\Lambda} := W^*_h \otimes S_\Lambda$, $\widetilde{\boldsymbol{V}}_{h,\Lambda} := \widetilde{\boldsymbol{V}}_h \otimes S_\Lambda$, $\widetilde{W}_{h,\Lambda} := \widetilde{W}_h \otimes S_\Lambda$, $\boldsymbol{V}_{h,\mathfrak{Q}} := \boldsymbol{V}_h \otimes S_\mathfrak{Q}$ and $W_{h,\mathfrak{Q}} := W_h \otimes S_\mathfrak{Q}$. The separation of the spatial and parametric detail spaces (the terms in brackets added to the current approximation spaces $\boldsymbol{V}_{h,\Lambda}$ and $W_{h,\Lambda}$) is the key idea underlying the error estimation strategy discussed in the next section.

4. A posteriori error estimation

We now want to estimate the SG-MFEM errors $\boldsymbol{e}^{\boldsymbol{u}} = \boldsymbol{u} - \boldsymbol{u}_{h,\Lambda}$, $e^p = p - p_{h,\Lambda}$ and $e^{\tilde{p}} = \tilde{p} - \tilde{p}_{h,\Lambda}$. To that end, we extend the *residual approach* described, e.g., in [26, Section 3] to our three-field formulation. We provide a detailed derivation in order to show how the constants in the bounds depend on the discrete inf–sup constant and on the variability in the Young modulus. Substituting $\boldsymbol{u}$, p and $\tilde{p}$ in (7) by $\boldsymbol{u}_{h,\Lambda} + e^{\boldsymbol{u}}$, $p_{h,\Lambda} + e^p$ and $\tilde{p}_{h,\Lambda} + e^{\tilde{p}}$, respectively, we conclude that $(e^{\boldsymbol{u}}, e^p, e^{\tilde{p}}) \in \boldsymbol{\mathcal{V}} \times \mathcal{W} \times \mathcal{W}$ satisfies

$$a(e^{\boldsymbol{u}}, \boldsymbol{v}) + b(\boldsymbol{v}, e^p) = \mathcal{R}^{\boldsymbol{u}}(\boldsymbol{v}) \quad \forall \boldsymbol{v} \in \boldsymbol{\mathcal{V}}, \tag{30a}$$

$$b(e^{\boldsymbol{u}}, q) - c(e^{\tilde{p}}, q) = \mathcal{R}^p(q) \quad \forall q \in \mathcal{W}, \tag{30b}$$

$$-c(e^p, \tilde{q}) + d(e^{\tilde{p}}, \tilde{q}) = \mathcal{R}^{\tilde{p}}(\tilde{q}) \quad \forall \tilde{q} \in \mathcal{W}, \tag{30c}$$

where the linear functionals $\mathcal{R}^{\boldsymbol{u}} : \boldsymbol{\mathcal{V}} \to \mathbb{R}$ and $\mathcal{R}^p, \mathcal{R}^{\tilde{p}} : \mathcal{W} \to \mathbb{R}$ are defined as

$$\mathcal{R}^{\boldsymbol{u}}(\boldsymbol{v}) := f(\boldsymbol{v}) - a(\boldsymbol{u}_{h,\Lambda}, \boldsymbol{v}) - b(\boldsymbol{v}, p_{h,\Lambda}) \quad \forall \boldsymbol{v} \in \boldsymbol{\mathcal{V}}, \tag{31a}$$

$$\mathcal{R}^p(q) := -b(\boldsymbol{u}_{h,\Lambda}, q) + c(\tilde{p}_{h,\Lambda}, q) \qquad \forall q \in \mathcal{W}, \tag{31b}$$

$$\mathcal{R}^{\tilde{p}}(\tilde{q}) := c(p_{h,\Lambda}, \tilde{q}) - d(\tilde{p}_{h,\Lambda}, \tilde{q}) \qquad \forall \tilde{q} \in \mathcal{W}. \tag{31c}$$

Clearly, these functionals represent the residuals associated with the current SG-MFEM approximation. For each one, we define a weighted dual norm as follows

$$\|\mathcal{R}^{\boldsymbol{u}}\|_* := \sup_{\boldsymbol{v}\in\boldsymbol{\mathcal{V}}\setminus\{0\}} \frac{|\mathcal{R}^{\boldsymbol{u}}(\boldsymbol{v})|}{\alpha^{1/2}\|\nabla\boldsymbol{v}\|_{\boldsymbol{\mathcal{W}}}}, \tag{32}$$

$$\|\mathcal{R}^{p}\|_* := \sup_{q\in\mathcal{W}\setminus\{0\}} \frac{|\mathcal{R}^{p}(q)|}{(\alpha^{-1}+(\alpha\beta)^{-1})^{1/2}\|q\|_{\mathcal{W}}}, \tag{33}$$

$$\|\mathcal{R}^{\tilde{p}}\|_* := \sup_{\tilde{q}\in\mathcal{W}\setminus\{0\}} \frac{|\mathcal{R}^{\tilde{p}}(\tilde{q})|}{(\alpha\beta)^{-1/2}\|\tilde{q}\|_{\mathcal{W}}}. \tag{34}$$

The next result establishes an equivalence between the norm of the SG-MFEM approximation error and the sum of the dual norms of the three residuals.

Theorem 4.1. *Let $(e^{\boldsymbol{u}}, e^p, e^{\tilde{p}}) \in \boldsymbol{\mathcal{V}}\times\mathcal{W}\times\mathcal{W}$ be the error in the SG-MFEM approximation $(\boldsymbol{u}_{h,\Lambda}, p_{h,\Lambda}, \tilde{p}_{h,\Lambda}) \in \boldsymbol{V}_{h,\Lambda}\times W_{h,\Lambda}\times W_{h,\Lambda}$ of the solution to (15). Then*

$$C_3\left(\|\mathcal{R}^{\boldsymbol{u}}\|_* + \|\mathcal{R}^{p}\|_* + \|\mathcal{R}^{\tilde{p}}\|_*\right) \le |||(e^{\boldsymbol{u}}, e^p, e^{\tilde{p}})||| \le C_4\left(\|\mathcal{R}^{\boldsymbol{u}}\|_* + \|\mathcal{R}^{p}\|_* + \|\mathcal{R}^{\tilde{p}}\|_*\right),$$

where $C_3 := \left(\sqrt{3}\max\left\{E_{\max}+\sqrt{d},\, 1+\sqrt{d}\right\}\right)^{-1}$, $C_4 := C_2/(C_1 E_{\min})$ and C_1 and C_2 are the constants in Lemma 2.1.

Proof. Since $(e^{\boldsymbol{u}}, e^p, e^{\tilde{p}}) \in \boldsymbol{\mathcal{V}}\times\mathcal{W}\times\mathcal{W}$, then from Lemma 2.1 there exists a $(\boldsymbol{v}, q, \tilde{q}) \in \boldsymbol{\mathcal{V}}\times\mathcal{W}\times\mathcal{W}$ with $|||(\boldsymbol{v}, q, \tilde{q})||| \le C_2\,|||(e^{\boldsymbol{u}}, e^p, e^{\tilde{p}})|||$ such that

$$C_1\, E_{\min}\, |||(e^{\boldsymbol{u}}, e^p, e^{\tilde{p}})|||^2 \le \mathcal{B}(e^{\boldsymbol{u}}, e^p, e^{\tilde{p}}; \boldsymbol{v}, q, \tilde{q}), \tag{35}$$

where C_1 and C_2 depend on $E_{\max}$, C_K and C_D. Hence, we have by (30)

$$C_1\, E_{\min}\, |||(e^{\boldsymbol{u}}, e^p, e^{\tilde{p}})|||^2 \le \mathcal{R}^{\boldsymbol{u}}(\boldsymbol{v}) + \mathcal{R}^{p}(q) + \mathcal{R}^{\tilde{p}}(\tilde{q}). \tag{36}$$

Moreover, using the definitions of the dual norms, we have

$$C_1 E_{\min}|||(e^{\boldsymbol{u}}, e^p, e^{\tilde{p}})|||^2 \le \left(\|\mathcal{R}^{\boldsymbol{u}}\|_* + \|\mathcal{R}^{p}\|_* + \|\mathcal{R}^{\tilde{p}}\|_*\right) C_2|||(e^{\boldsymbol{u}}, e^p, e^{\tilde{p}})|||. \tag{37}$$

This establishes the upper bound. To establish the lower bound, we use the definition

$$\|\mathcal{R}^{\boldsymbol{u}}\|_* := \sup_{\boldsymbol{v}\in\boldsymbol{\mathcal{V}}\setminus\{0\}} \frac{|\mathcal{R}^{\boldsymbol{u}}(\boldsymbol{v})|}{\alpha^{1/2}\|\nabla\boldsymbol{v}\|_{\boldsymbol{\mathcal{W}}}} = \sup_{\boldsymbol{v}\in\boldsymbol{\mathcal{V}}\setminus\{0\}} \frac{|a(e^{\boldsymbol{u}}, \boldsymbol{v}) + b(\boldsymbol{v}, e^p)|}{\alpha^{1/2}\|\nabla\boldsymbol{v}\|_{\boldsymbol{\mathcal{W}}}}, \tag{38}$$

and simply bound the two bilinear forms separately

$$\|\mathcal{R}^{\boldsymbol{u}}\|_* \le E_{\max}\alpha^{1/2}\|\nabla e^{\boldsymbol{u}}\|_{\boldsymbol{\mathcal{W}}} + \sqrt{d}\alpha^{-1/2}\|e^p\|_{\mathcal{W}}. \tag{39}$$

Similarly, noting that $(\alpha^{-1}+(\alpha\beta)^{-1})^{-1/2} \le \alpha^{1/2}$ and $(\alpha\beta)^{-1}(\alpha^{-1}+(\alpha\beta)^{-1})^{-1/2} \le (\alpha\beta)^{-1/2}$, we deduce that

$$\|\mathcal{R}^{p}\|_* \le \sqrt{d}\alpha^{1/2}\|\nabla e^{\boldsymbol{u}}\|_{\boldsymbol{\mathcal{W}}} + (\alpha\beta)^{-1/2}\|e^{\tilde{p}}\|_{\mathcal{W}}, \tag{40}$$

$$\|\mathcal{R}^{\tilde{p}}\|_* \le\ (\alpha\beta)^{-1/2}\|e^p\|_{\mathcal{W}} + E_{\max}(\alpha\beta)^{-1/2}\|e^{\tilde{p}}\|_{\mathcal{W}}. \tag{41}$$

Combining (39), (40) and (41), and recalling the definition of the norm $|||(\cdot,\cdot,\cdot)|||$ in (16) implies the stated result. □

Theorem 4.1 is our starting point for developing an a posteriori error estimation strategy. We will estimate $|||(e^{\boldsymbol{u}}, e^p, e^{\tilde{p}})|||$ by estimating $\|\mathcal{R}^{\boldsymbol{u}}\|_* + \|\mathcal{R}^{p}\|_* + \|\mathcal{R}^{\tilde{p}}\|_*$.

4.1. **Fast evaluation of the residuals.** First, we give an alternative representation of each of $\|\mathcal{R}^{\boldsymbol{u}}\|_*$, $\|\mathcal{R}^p\|_*$ and $\|\mathcal{R}^{\tilde{p}}\|_*$ and show that $\|\mathcal{R}^p\|_*$ can be evaluated exactly. Since $\boldsymbol{\mathcal{V}}$ and $\mathcal{W}$ are Hilbert spaces, the Riesz representation theorem tells us that we can find a unique $\boldsymbol{e}_0^{\boldsymbol{u}} \in \boldsymbol{\mathcal{V}}$, a unique $e_0^p \in \mathcal{W}$ and a unique $e_0^{\tilde{p}} \in \mathcal{W}$ such that

$$\bar{a}_0(\boldsymbol{e}_0^{\boldsymbol{u}}, \boldsymbol{v}) = \mathcal{R}^{\boldsymbol{u}}(\boldsymbol{v}) \qquad \forall \boldsymbol{v} \in \boldsymbol{\mathcal{V}}, \tag{42a}$$

$$\bar{c}(e_0^p, q) = \mathcal{R}^p(q) \qquad \forall q \in \mathcal{W}, \tag{42b}$$

$$\bar{d}_0(e_0^{\tilde{p}}, \tilde{q}) = \mathcal{R}^{\tilde{p}}(\tilde{q}) \qquad \forall \tilde{q} \in \mathcal{W}, \tag{42c}$$

where, for efficient computation (the complexity of the resulting linear algebra is significantly reduced) we simply use the parameter-free inner products

$$\bar{a}_0(\boldsymbol{u}, \boldsymbol{v}) := \alpha \int_\Gamma \int_D \nabla \boldsymbol{u}(\boldsymbol{x}, \boldsymbol{y}) : \nabla \boldsymbol{v}(\boldsymbol{x}, \boldsymbol{y}) \, d\boldsymbol{x} \, d\pi(\boldsymbol{y}), \tag{43}$$

$$\bar{c}(p, q) := \left(\alpha^{-1} + (\alpha\beta)^{-1}\right) \int_\Gamma \int_D p(\boldsymbol{x}, \boldsymbol{y}) q(\boldsymbol{x}, \boldsymbol{y}) \, d\boldsymbol{x} \, d\pi(\boldsymbol{y}), \tag{44}$$

$$\bar{d}_0(p, q) := (\alpha\beta)^{-1} \int_\Gamma \int_D p(\boldsymbol{x}, \boldsymbol{y}) q(\boldsymbol{x}, \boldsymbol{y}) \, d\boldsymbol{x} \, d\pi(\boldsymbol{y}). \tag{45}$$

Note that $\bar{d}_0(\cdot, \cdot)$ is identical to $c(\cdot, \cdot)$ in (10). We use the notation $\bar{d}_0(\cdot, \cdot)$ to emphasise that it is an approximation to the bilinear form $d(\cdot, \cdot)$ defined in (11). Similarly, $\bar{a}_0(\cdot, \cdot)$ represents $a(\cdot, \cdot)$ in (8) with the strain energy approximated by the Dirichlet energy. We observe that

$$|\boldsymbol{e}_0^{\boldsymbol{u}}|_{\bar{a}_0} := \sqrt{\bar{a}_0(\boldsymbol{e}_0^{\boldsymbol{u}}, \boldsymbol{e}_0^{\boldsymbol{u}})} = \|\mathcal{R}^{\boldsymbol{u}}\|_*, \tag{46}$$

$$|e_0^p|_{\bar{c}} := \sqrt{\bar{c}(e_0^p, e_0^p)} = \|\mathcal{R}^p\|_*, \tag{47}$$

$$|e_0^{\tilde{p}}|_{\bar{d}_0} := \sqrt{\bar{d}_0(e_0^{\tilde{p}}, e_0^{\tilde{p}})} = \|\mathcal{R}^{\tilde{p}}\|_*. \tag{48}$$

Note that

$$|||(\boldsymbol{v}, p, \tilde{p})|||^2 = |\boldsymbol{v}|_{\bar{a}_0}^2 + |p|_{\bar{c}}^2 + |\tilde{p}|_{\bar{d}_0}^2, \quad |(\boldsymbol{v}, p, \tilde{p}) \in \boldsymbol{\mathcal{V}} \times \mathcal{W} \times \mathcal{W}.$$

Now, from (42b) and the definition of $\mathcal{R}^p$ in (31b), $\bar{c}(e_0^p, q) = -b(\boldsymbol{u}_{h,\Lambda}, q) + c(\tilde{p}_{h,\Lambda}, q)$ for all $q \in \mathcal{W}$, from which we conclude that

$$e_0^p = (\alpha^{-1} + (\alpha\beta)^{-1})^{-1}(\nabla \cdot \boldsymbol{u}_{h,\Lambda} + (\alpha\beta)^{-1}\tilde{p}_{h,\Lambda}) \quad \text{a.e. in } D \times \Gamma. \tag{49}$$

Hence, unlike $\|\mathcal{R}^{\boldsymbol{u}}\|_*$ and $\|\mathcal{R}^{\tilde{p}}\|_*$, we can compute $\|\mathcal{R}^p\|_* = |e_0^p|_{\bar{c}}$ directly. This is due to the fact that $\mathcal{R}^p$ only involves the bilinear forms $b(\cdot, \cdot)$ and $c(\cdot, \cdot)$, neither of which include the parametric Young's modulus E.

4.2. **Approximation of the residuals.** We can now approximate the solutions $\boldsymbol{e}_0^{\boldsymbol{u}}$ and $e_0^{\tilde{p}}$ to (42a) and (42c) by replacing the infinite-dimensional spaces $\boldsymbol{\mathcal{V}}$ and $\mathcal{W}$ with finite-dimensional ones. This will be done using the hierarchical construction introduced in the previous section. Thus, recalling the definitions of the spaces $\boldsymbol{V}_{h,\Lambda}^* \subset \boldsymbol{\mathcal{V}}$ and $W_{h,\Lambda}^* \subset \mathcal{W}$ in (28) and (29), we consider the problems: find $\boldsymbol{e}_0^{\boldsymbol{u},*} \in \boldsymbol{V}_{h,\Lambda}^*$ and $e_0^{\tilde{p},*} \in W_{h,\Lambda}^*$ such that

$$\bar{a}_0(\boldsymbol{e}_0^{\boldsymbol{u},*}, \boldsymbol{v}) = \mathcal{R}^{\boldsymbol{u}}(\boldsymbol{v}) \qquad \forall \boldsymbol{v} \in \boldsymbol{V}_{h,\Lambda}^*, \tag{50a}$$

$$\bar{d}_0(e_0^{\tilde{p},*}, \tilde{q}) = \mathcal{R}^{\tilde{p}}(\tilde{q}) \qquad \forall \tilde{q} \in W_{h,\Lambda}^*. \tag{50b}$$

From (42a) and (50a), we have

$$\bar{a}_0(\boldsymbol{e}_0^{\boldsymbol{u}} - \boldsymbol{e}_0^{\boldsymbol{u},*}, \boldsymbol{v}) = 0 \quad \forall \boldsymbol{v} \in \boldsymbol{V}_{h,\Lambda}^*,$$

and similarly,

$$\bar{d}_0(e_0^{\tilde{p}} - e_0^{\tilde{p},*}, \tilde{q}) = 0 \qquad \forall \tilde{q} \in W_{h,\Lambda}^*.$$

Hence, $\boldsymbol{e}_0^{\boldsymbol{u},*}$ is simply the orthogonal projection of $\boldsymbol{e}_0^{\boldsymbol{u}}$ onto the space $\boldsymbol{V}_{h,\Lambda}^*$ with respect to the inner product $\bar{a}_0(\cdot,\cdot)$, and $e_0^{\tilde{p},*}$ is the orthogonal projection of $e_0^{\tilde{p}}$ onto the space $W_{h,\Lambda}^*$ with respect to $\bar{d}_0(\cdot,\cdot)$. As a consequence of this, we have

$$|\boldsymbol{e}_0^{\boldsymbol{u},*}|_{\bar{a}_0}^2 + |\boldsymbol{e}_0^{\boldsymbol{u}} - \boldsymbol{e}_0^{\boldsymbol{u},*}|_{\bar{a}_0}^2 = |\boldsymbol{e}_0^{\boldsymbol{u}}|_{\bar{a}_0}^2, \quad |e_0^{\tilde{p},*}|_{\bar{d}_0}^2 + |e_0^{\tilde{p}} - e_0^{\tilde{p},*}|_{\bar{d}_0}^2 = |e_0^{\tilde{p}}|_{\bar{d}_0}^2, \tag{51}$$

which gives

$$|\boldsymbol{e}_0^{\boldsymbol{u}} - \boldsymbol{e}_0^{\boldsymbol{u},*}|_{\bar{a}_0}^2 \leq |\boldsymbol{e}_0^{\boldsymbol{u}}|_{\bar{a}_0}^2, \quad |e_0^{\tilde{p}} - e_0^{\tilde{p},*}|_{\bar{d}_0}^2 \leq |e_0^{\tilde{p}}|_{\bar{d}_0}^2. \tag{52}$$

From this point onwards we suppose that the rules $\boldsymbol{V}_{h,\Lambda} \to \boldsymbol{V}_{h,\Lambda}^*$ and $W_{h,\Lambda} \to W_{h,\Lambda}^*$ are fixed. An adaptive refinement strategy will be presented later. The following saturation assumption will be needed if we want to ensure that the estimated error will decrease at every step of the refinement process.

Assumption 4.1. *There exists a constant $\Theta \in [0,1)$ that is independent of h and Λ such that*

$$|\boldsymbol{e}_0^{\boldsymbol{u}} - \boldsymbol{e}_0^{\boldsymbol{u},*}|_{\bar{a}_0} \leq \Theta\, |\boldsymbol{e}_0^{\boldsymbol{u}}|_{\bar{a}_0}, \quad |e_0^{\tilde{p}} - e_0^{\tilde{p},*}|_{\bar{d}_0} \leq \Theta\, |e_0^{\tilde{p}}|_{\bar{d}_0}. \tag{53}$$

Lemma 4.2. *Let $\boldsymbol{e}_0^{\boldsymbol{u}} \in \boldsymbol{\mathcal{V}}$ and $e_0^{\tilde{p}} \in \mathcal{W}$ satisfy* (42a) *and* (42c) *and let $\boldsymbol{e}_0^{\boldsymbol{u},*} \in \boldsymbol{V}_{h,\Lambda}^*$ and $e_0^{\tilde{p},*} \in W_{h,\Lambda}^*$ satisfy Assumption 4.1. Then,*

$$|\boldsymbol{e}_0^{\boldsymbol{u},*}|_{\bar{a}_0} \leq |\boldsymbol{e}_0^{\boldsymbol{u}}|_{\bar{a}_0} \leq \frac{1}{\sqrt{1-\Theta^2}} |\boldsymbol{e}_0^{\boldsymbol{u},*}|_{\bar{a}_0}, \tag{54a}$$

$$|e_0^{\tilde{p},*}|_{\bar{d}_0} \leq |e_0^{\tilde{p}}|_{\bar{d}_0} \leq \frac{1}{\sqrt{1-\Theta^2}} |e_0^{\tilde{p},*}|_{\bar{d}_0}, \tag{54b}$$

where Θ is the constant in (53).

Proof. The left-hand-side inequalities in (54) follow directly from (51). Using (51) and squaring both sides of the equations in (53) gives

$$|\boldsymbol{e}_0^{\boldsymbol{u}}|_{\bar{a}_0}^2 - |\boldsymbol{e}_0^{\boldsymbol{u},*}|_{\bar{a}_0}^2 = |\boldsymbol{e}_0^{\boldsymbol{u}} - \boldsymbol{e}_0^{\boldsymbol{u},*}|_{\bar{a}_0}^2 \leq \Theta^2 |\boldsymbol{e}_0^{\boldsymbol{u}}|_{\bar{a}_0}^2, \tag{55a}$$

$$|e_0^{\tilde{p}}|_{\bar{d}_0}^2 - |e_0^{\tilde{p},*}|_{\bar{d}_0}^2 = |e_0^{\tilde{p}} - e_0^{\tilde{p},*}|_{\bar{d}_0}^2 \leq \Theta^2 |e_0^{\tilde{p}}|_{\bar{d}_0}^2, \tag{55b}$$

which proves the right-hand-side inequalities in (54). □

Although the estimates $|\boldsymbol{e}_0^{\boldsymbol{u},*}|_{\bar{a}_0}$ and $|e_0^{\tilde{p},*}|_{\bar{d}_0}$ are computable, the dimensions of $\boldsymbol{V}_{h,\Lambda}^*$ and $W_{h,\Lambda}^*$ may be much larger than those of $\boldsymbol{V}_{h,\Lambda}$ and $W_{h,\Lambda}$. Fortunately, we can exploit the structure shown in (28) and (29) to obtain lower-dimensional problems, leading to estimates that are cheaper to compute. Specifically, instead of solving (50a) and (50b), we consider the *detail space* problems: find $\boldsymbol{e}_2^{\boldsymbol{u}} \in \widetilde{\boldsymbol{V}}_{h,\Lambda} \oplus \boldsymbol{V}_{h,\mathfrak{Q}}$ and $e_2^{\tilde{p}} \in \widetilde{W}_{h,\Lambda} \oplus W_{h,\mathfrak{Q}}$ such that

$$\bar{a}_0(\boldsymbol{e}_2^{\boldsymbol{u}}, \boldsymbol{v}) = \mathcal{R}^{\boldsymbol{u}}(\boldsymbol{v}) \qquad \forall \boldsymbol{v} \in \widetilde{\boldsymbol{V}}_{h,\Lambda} \oplus \boldsymbol{V}_{h,\mathfrak{Q}}, \tag{56a}$$

$$\bar{d}_0(e_2^{\tilde{p}}, \tilde{q}) = \mathcal{R}^{\tilde{p}}(\tilde{q}) \qquad \forall \tilde{q} \in \widetilde{W}_{h,\Lambda} \oplus W_{h,\mathfrak{Q}}. \tag{56b}$$

We also define the error estimates

$$\eta_1 := |\boldsymbol{e}_2^{\boldsymbol{u}}|_{\bar{a}_0}, \quad \eta_2 := |e_0^p|_{\bar{c}}, \quad \eta_3 := |e_2^{\tilde{p}}|_{\bar{d}_0}, \tag{57}$$

where we recall that e_0^p is given directly by (49).

To compute these estimates, we introduce the decompositions

$$\boldsymbol{e}_2^{\boldsymbol{u}} = \tilde{\boldsymbol{e}}_{h,\Lambda}^{\boldsymbol{u}} + \boldsymbol{e}_{h,\mathfrak{Q}}^{\boldsymbol{u}}, \quad e_2^{\tilde{p}} = \tilde{e}_{h,\Lambda}^{\tilde{p}} + e_{h,\mathfrak{Q}}^{\tilde{p}}, \tag{58}$$

where $\tilde{\boldsymbol{e}}_{h,\Lambda}^{\boldsymbol{u}} \in \widetilde{\boldsymbol{V}}_{h,\Lambda}$, $\boldsymbol{e}_{h,\mathfrak{Q}}^{\boldsymbol{u}} \in \boldsymbol{V}_{h,\mathfrak{Q}}$, $\tilde{e}_{h,\Lambda}^{\tilde{p}} \in \widetilde{W}_{h,\Lambda}$, and $e_{h,\mathfrak{Q}}^{\tilde{p}} \in W_{h,\mathfrak{Q}}$. Choosing test functions $\boldsymbol{v} \in \widetilde{\boldsymbol{V}}_{h,\Lambda}$ in (56a) and $\tilde{q} \in \widetilde{W}_{h,\Lambda}$ in (56b) and using the orthogonality of the polynomials in S_Λ and $S_\mathfrak{Q}$ with respect to the measure π gives

$$\bar{a}_0(\tilde{\boldsymbol{e}}_{h,\Lambda}^{\boldsymbol{u}}, \boldsymbol{v}) = \mathcal{R}^{\boldsymbol{u}}(\boldsymbol{v}) \quad \forall \boldsymbol{v} \in \widetilde{\boldsymbol{V}}_{h,\Lambda}, \tag{59a}$$

$$\bar{d}_0(\tilde{e}_{h,\Lambda}^{\tilde{p}}, \tilde{q}) = \mathcal{R}^{\tilde{p}}(\tilde{q}) \quad \forall \tilde{q} \in \widetilde{W}_{h,\Lambda}. \tag{59b}$$

We will refer to $\tilde{\boldsymbol{e}}_{h,\Lambda}^{\boldsymbol{u}}$ and $\tilde{e}_{h,\Lambda}^{\tilde{p}}$ as the *spatial* error estimators. Similarly, choosing test functions $\boldsymbol{v} \in \boldsymbol{V}_{h,\mathfrak{Q}}$ in (56a) and $\tilde{q} \in W_{h,\mathfrak{Q}}$ in (56b) gives

$$\bar{a}_0(\boldsymbol{e}_{h,\mathfrak{Q}}^{\boldsymbol{u}}, \boldsymbol{v}) = \mathcal{R}^{\boldsymbol{u}}(\boldsymbol{v}) \quad \forall \boldsymbol{v} \in \boldsymbol{V}_{h,\mathfrak{Q}}, \tag{60a}$$

$$\bar{d}_0(e_{h,\mathfrak{Q}}^{\tilde{p}}, \tilde{q}) = \mathcal{R}^{\tilde{p}}(\tilde{q}) \quad \forall \tilde{q} \in W_{h,\mathfrak{Q}}. \tag{60b}$$

We will refer to $\boldsymbol{e}_{h,\mathfrak{Q}}^{\boldsymbol{u}}$ and $e_{h,\mathfrak{Q}}^{\tilde{p}}$ as the *parametric* error estimators.

Since $\bar{a}_0(\tilde{\boldsymbol{e}}_{h,\Lambda}^{\boldsymbol{u}}, \boldsymbol{e}_{h,\mathfrak{Q}}^{\boldsymbol{u}}) = 0$ and $\bar{d}_0(\tilde{e}_{h,\Lambda}^{\tilde{p}}, e_{h,\mathfrak{Q}}^{\tilde{p}}) = 0$, we can write η_1 and η_3 as

$$\eta_1 = |\tilde{\boldsymbol{e}}_{h,\Lambda}^{\boldsymbol{u}} + \boldsymbol{e}_{h,\mathfrak{Q}}^{\boldsymbol{u}}|_{\bar{a}_0} = (|\tilde{\boldsymbol{e}}_{h,\Lambda}^{\boldsymbol{u}}|_{\bar{a}_0}^2 + |\boldsymbol{e}_{h,\mathfrak{Q}}^{\boldsymbol{u}}|_{\bar{a}_0}^2)^{1/2}, \tag{61}$$

$$\eta_3 = |\tilde{e}_{h,\Lambda}^{\tilde{p}} + e_{h,\mathfrak{Q}}^{\tilde{p}}|_{\bar{d}_0} = (|\tilde{e}_{h,\Lambda}^{\tilde{p}}|_{\bar{d}_0}^2 + |e_{h,\mathfrak{Q}}^{\tilde{p}}|_{\bar{d}_0}^2)^{1/2}. \tag{62}$$

Thus, in summary, to compute η_1 and η_3, we need to solve four decoupled detail space problems (59a)–(60b). The following result characterises how well η_1 and η_3 approximate $|\boldsymbol{e}_0^{\boldsymbol{u},*}|_{\bar{a}_0}$ and $|e_0^{\tilde{p},*}|_{\bar{d}_0}$, respectively.

Lemma 4.3. *Let $e_0^{\boldsymbol{u},*} \in \boldsymbol{V}_{h,\Lambda}^*$ and $e_0^{\tilde{p},*} \in W_{h,\Lambda}^*$ satisfy* (50)*. Let the error estimates η_1 and η_3 be as given in* (61) *and* (62)*. Then,*

$$\eta_1 \le |\boldsymbol{e}_0^{\boldsymbol{u},*}|_{\bar{a}_0} \le \frac{1}{\sqrt{1-\gamma_1^2}}\,\eta_1, \qquad \eta_3 \le |e_0^{\tilde{p},*}|_{\bar{d}_0} \le \frac{1}{\sqrt{1-\gamma_2^2}}\,\eta_3, \tag{63}$$

where γ_1 and γ_2 are the CBS constants from (26a) *and* (26b) *respectively.*

Proof. This involves a standard argument. The construction can be found in the proof of Lemma 2.1 in [7]. □

Combining the individual error estimates in (57) gives the total error estimate

$$\eta := (\eta_1^2 + \eta_2^2 + \eta_3^2)^{1/2}. \tag{64}$$

The equivalence between η and the true error is summarised in the following result.

Theorem 4.4. *Let $(e^{\boldsymbol{u}}, e^p, e^{\tilde{p}}) \in \boldsymbol{\mathcal{V}} \times \mathcal{W} \times \mathcal{W}$ be the error in the approximation $(\boldsymbol{u}_{h,\Lambda}, p_{h,\Lambda}, \tilde{p}_{h,\Lambda}) \in \boldsymbol{V}_{h,\Lambda} \times W_{h,\Lambda} \times W_{h,\Lambda}$ of the solution to* (15) *and suppose that Assumption 4.1 holds. Then*

$$C_3\,\eta \le |||(e^{\boldsymbol{u}}, e^p, e^{\tilde{p}})||| \le \frac{C_4}{\sqrt{1-\gamma^2}\sqrt{1-\Theta^2}}\,\eta, \tag{65}$$

where C_3 and C_4 are defined in Theorem 4.1, $\gamma \in [0,1)$ is the larger of the two CBS constants in (26)*, and $\Theta \in [0,1)$ is the saturation constant in* (53)*.*

Proof. Combining the bounds in Theorem 4.1, Lemma 4.2 and Lemma 4.3 leads to the stated result. □

The following corollary will be useful in the numerical results section.

Corollary 4.5. *Let* $(e^{\boldsymbol{u}}, e^p, e^{\tilde{p}}) \in \boldsymbol{\mathcal{V}} \times \mathcal{W} \times \mathcal{W}$ *be the error in the approximation* $(\boldsymbol{u}_{h,\Lambda}, p_{h,\Lambda}, \tilde{p}_{h,\Lambda}) \in \boldsymbol{V}_{h,\Lambda} \times W_{h,\Lambda} \times W_{h,\Lambda}$ *of the solution to* (15)*. Then*

$$\mathcal{E} \leq \frac{C_4}{\sqrt{1-\gamma^2}\sqrt{1-\Theta^2}}\eta, \tag{66}$$

where

$$\mathcal{E} := \sqrt{\alpha\|\mathbb{E}(\nabla \boldsymbol{e}^{\boldsymbol{u}})\|^2_{L^2(D)} + (\alpha^{-1} + (\alpha\beta)^{-1})\|\mathbb{E}(e^p)\|^2_{L^2(D)} + (\alpha\beta)^{-1}\|\mathbb{E}(e^{\tilde{p}})\|^2_{L^2(D)}}$$

defines a surrogate energy norm that is much easier to compute.

Proof. The proof directly follows from Theorem 4.4, using Jensen's inequality and the definition of the norm $|||\cdot|||$ in (16). □

4.3. **The incompressible limit case.** If $\nu = \frac{1}{2}$, then our three-field formulation (2) reduces to the following two-field formulation representing the Stokes problem: find $\boldsymbol{u} : D \times \Gamma \to \mathbb{R}^d$ and $p : D \times \Gamma \to \mathbb{R}$ such that

$$-\nabla \cdot \boldsymbol{\sigma}(\boldsymbol{x}, \boldsymbol{y}) = \boldsymbol{f}(\boldsymbol{x}), \quad \boldsymbol{x} \in D,\ \boldsymbol{y} \in \Gamma, \tag{67a}$$

$$\nabla \cdot \boldsymbol{u}(\boldsymbol{x}, \boldsymbol{y}) = 0, \qquad \boldsymbol{x} \in D,\ \boldsymbol{y} \in \Gamma, \tag{67b}$$

$$\boldsymbol{u}(\boldsymbol{x}, \boldsymbol{y}) = \boldsymbol{g}(\boldsymbol{x}), \quad \boldsymbol{x} \in \partial D_D,\ \boldsymbol{y} \in \Gamma, \tag{67c}$$

$$\boldsymbol{\sigma}(\boldsymbol{x}, \boldsymbol{y})\, \boldsymbol{n} = \boldsymbol{0}, \qquad \boldsymbol{x} \in \partial D_N,\ \boldsymbol{y} \in \Gamma. \tag{67d}$$

Assuming that $\boldsymbol{f} \in \boldsymbol{L}^2(D)$ and $\boldsymbol{g} = \boldsymbol{0}$ on ∂D_D, the weak formulation of (67) and the associated SG-MFEM formulation follow from (7) and (22), respectively, by formally setting the bilinear forms $c(\cdot,\cdot)$ and $d(\cdot,\cdot)$ to zero and omitting the third components of the weak and Galerkin solutions. In the incompressible limit, the error estimate η defined in (64) becomes $\eta = (\eta_1^2 + \eta_2^2)^{1/2}$, where η_1 and η_2 are given in (57) (with $\eta_2 = \alpha^{1/2}\|\nabla \cdot \boldsymbol{u}_{h,\Lambda}\|_{\mathcal{W}}$). The following error bound is an immediate consequence of Theorem 4.4.

Theorem 4.6. *Let* $(\boldsymbol{e}^{\boldsymbol{u}}, e^p)$ *be the error in the Galerkin approximation of the solution to the Stokes problem* (67) *and suppose that Assumption 4.1 holds. Then*

$$C_3\,\eta \leq |||(\boldsymbol{e}^{\boldsymbol{u}}, e^p)|||_S \leq \frac{C_4}{\sqrt{1-\gamma^2}\sqrt{1-\Theta^2}}\eta, \tag{68}$$

where $|||(\boldsymbol{v}, q)|||_S^2 := \alpha\|\nabla \boldsymbol{v}\|^2_{\boldsymbol{\mathcal{W}}} + \alpha^{-1}\|q\|^2_{\mathcal{W}}$, $C_3 := \big(\sqrt{2}(E_{\max} + \sqrt{d})\big)^{-1}$ *with constants* C_4, γ *and* Θ *given in Theorem 4.4.*

5. Proxies for the potential error reduction in an adaptive setting

Recall that the *spatial* error estimators $\tilde{\boldsymbol{e}}^{\boldsymbol{u}}_{h,\Lambda} \in \widetilde{\boldsymbol{V}}_{h,\Lambda}$ and $\tilde{e}^{\tilde{p}}_{h,\Lambda} \in \widetilde{W}_{h,\Lambda}$ contributing to η_1 and η_3 satisfy (59a) and (59b), respectively, and that the *parametric* error estimators $\boldsymbol{e}^{\boldsymbol{u}}_{h,\mathfrak{Q}} \in \boldsymbol{V}_{h,\mathfrak{Q}}$ and $e^{\tilde{p}}_{h,\mathfrak{Q}} \in W_{h,\mathfrak{Q}}$ satisfy (60a) and (60b). Let us also define a *third* spatial error estimator $\tilde{e}^{p}_{h,\Lambda} \in \widetilde{W}_{h,\Lambda}$ that satisfies

$$\bar{c}(\tilde{e}^{p}_{h,\Lambda}, q) = \mathcal{R}^p(q) \quad \forall q \in \widetilde{W}_{h,\Lambda}. \tag{69}$$

Combining the three spatial error estimators and the two parametric error estimators gives

$$\eta_{h^*,\Lambda} := \big(|\tilde{\boldsymbol{e}}^{\boldsymbol{u}}_{h,\Lambda}|^2_{\bar{a}_0} + |\tilde{e}^{p}_{h,\Lambda}|^2_{\bar{c}} + |\tilde{e}^{\tilde{p}}_{h,\Lambda}|^2_{\bar{d}_0}\big)^{1/2}, \tag{70a}$$

$$\eta_{h,\mathfrak{Q}} := \big(|\boldsymbol{e}^{\boldsymbol{u}}_{h,\mathfrak{Q}}|^2_{\bar{a}_0} + |e^{\tilde{p}}_{h,\mathfrak{Q}}|^2_{\bar{d}_0}\big)^{1/2}. \tag{70b}$$

We will use these as error reduction proxies within an adaptive refinement scheme.

To simplify notation, let $\mathcal{U} := (\boldsymbol{u}, p, \tilde{p}) \in \boldsymbol{\mathcal{V}} \times \mathcal{W} \times \mathcal{W}$ denote the exact solution to (15) and let $\mathcal{U}_{h,\Lambda} := (\boldsymbol{u}_{h,\Lambda}, p_{h,\Lambda}, \tilde{p}_{h,\Lambda}) \in \boldsymbol{V}_{h,\Lambda} \times W_{h,\Lambda} \times W_{h,\Lambda}$ denote the SG-MFEM approximation. Similarly, let $\mathcal{U}_{h^*,\Lambda} := (\boldsymbol{u}_{h^*,\Lambda}, p_{h^*,\Lambda}, \tilde{p}_{h^*,\Lambda}) \in \boldsymbol{V}_{h^*,\Lambda} \times W_{h^*,\Lambda} \times W_{h^*,\Lambda}$ (resp., $\mathcal{U}_{h,\Lambda^*} := (\boldsymbol{u}_{h,\Lambda^*}, p_{h,\Lambda^*}, \tilde{p}_{h,\Lambda^*}) \in \boldsymbol{V}_{h,\Lambda^*} \times W_{h,\Lambda^*} \times W_{h,\Lambda^*}$) denote the enhanced SG-MFEM approximation corresponding to the pair $\boldsymbol{V}_h^*$–W_h^* of enriched finite element spaces (resp., the enriched polynomial space S^*_Λ). From the triangle inequality we have

$$|||\mathcal{U} - \mathcal{U}_{h,\Lambda}||| - |||\mathcal{U} - \mathcal{U}_{h^*,\Lambda}||| \le |||\mathcal{U}_{h^*,\Lambda} - \mathcal{U}_{h,\Lambda}|||.$$

Thus, we can quantify the potential reduction in the $|||\cdot|||$-norm of the error that would be achieved by enriching the finite element spaces, by estimating the quantity $|||\mathcal{U}_{h^*,\Lambda} - \mathcal{U}_{h,\Lambda}|||$. Similarly, we can quantify the potential reduction that would be achieved by enriching the polynomial space for the parametric part, by estimating $|||\mathcal{U}_{h,\Lambda^*} - \mathcal{U}_{h,\Lambda}|||$. The next result shows that $\eta_{h^*,\Lambda}$ and $\eta_{h,\mathfrak{Q}}$ provide reliable and efficient proxies for $|||\mathcal{U}_{h^*,\Lambda} - \mathcal{U}_{h,\Lambda}|||$ and $|||\mathcal{U}_{h,\Lambda^*} - \mathcal{U}_{h,\Lambda}|||$, respectively.

Theorem 5.1. *Let $\mathcal{U}_{h,\Lambda} \in \boldsymbol{V}_{h,\Lambda} \times W_{h,\Lambda} \times W_{h,\Lambda}$ be the approximation of the solution to* (15) *and let $\mathcal{U}_{h^*,\Lambda} \in \boldsymbol{V}_{h^*,\Lambda} \times W_{h^*,\Lambda} \times W_{h^*,\Lambda}$ and $\mathcal{U}_{h,\Lambda^*} \in \boldsymbol{V}_{h,\Lambda^*} \times W_{h,\Lambda^*} \times W_{h,\Lambda^*}$ denote the SG-MFEM approximations as defined above. Then,*

$$C_3\, \eta_{h^*,\Lambda} \le |||\mathcal{U}_{h^*,\Lambda} - \mathcal{U}_{h,\Lambda}||| \le \frac{\widehat{C}_4}{\sqrt{1-\gamma^2}}\, \eta_{h^*,\Lambda}, \tag{71}$$

$$C_3\, \eta_{h,\mathfrak{Q}} \le |||\mathcal{U}_{h,\Lambda^*} - \mathcal{U}_{h,\Lambda}||| \le \widehat{C}_4\, \eta_{h,\mathfrak{Q}}, \tag{72}$$

where $\widehat{C}_4 := \frac{\widehat{C}_2}{\widehat{C}_1 E_{\min}}$. The constants $\widehat{C}_1$ and $\widehat{C}_2$ are defined similarly to C_1^* and C_2^* in Lemma 3.1, with γ_h replaced by the inf–sup constant associated with the finite element spaces $\boldsymbol{V}_h^*$ and W_h^*. The constant C_3 is given in Theorem 4.1 and $\gamma \in [0,1)$ is the CBS constant in Theorem 4.4.

Proof. Let us prove (71), the proof of (72) proceeds in the same way. The enhanced approximation $\mathcal{U}_{h^*,\Lambda} = (\boldsymbol{u}_{h^*,\Lambda}, p_{h^*,\Lambda}, \tilde{p}_{h^*,\Lambda})$ satisfies

$$a(\boldsymbol{u}_{h^*,\Lambda}, \boldsymbol{v}) + b(\boldsymbol{v}, p_{h^*,\Lambda}) = f(\boldsymbol{v}) \qquad \forall \boldsymbol{v} \in \boldsymbol{V}_{h^*,\Lambda}, \tag{73a}$$

$$b(\boldsymbol{u}_{h^*,\Lambda}, q) - c(\tilde{p}_{h^*,\Lambda}, q) = 0 \qquad \forall q \in W_{h^*,\Lambda}, \tag{73b}$$

$$-c(p_{h^*,\Lambda}, r) + d(\tilde{p}_{h^*,\Lambda}, r) = 0 \qquad \forall r \in W_{h^*,\Lambda}. \tag{73c}$$

Recalling the definitions of the residual functionals in (31) and combining (59), (69) and (73) implies

$$\bar{a}_0(\tilde{\boldsymbol{e}}^{\boldsymbol{u}}_{h,\Lambda}, \boldsymbol{v}) = a(\boldsymbol{u}_{h^*,\Lambda} - \boldsymbol{u}_{h,\Lambda}, \boldsymbol{v}) + b(\boldsymbol{v}, p_{h^*,\Lambda} - p_{h,\Lambda}) \quad \forall \boldsymbol{v} \in \widetilde{\boldsymbol{V}}_{h,\Lambda}, \tag{74a}$$

$$\bar{c}(\tilde{e}^{p}_{h,\Lambda}, q) = b(\boldsymbol{u}_{h^*,\Lambda} - \boldsymbol{u}_{h,\Lambda}, q) - c(\tilde{p}_{h^*,\Lambda} - \tilde{p}_{h,\Lambda}, q) \quad \forall q \in \widetilde{W}_{h,\Lambda}, \tag{74b}$$

$$\bar{d}_0(\tilde{e}^{\tilde{p}}_{h,\Lambda}, r) = -c(p_{h^*,\Lambda} - p_{h,\Lambda}, r) + d(\tilde{p}_{h^*,\Lambda} - \tilde{p}_{h,\Lambda}, r) \quad \forall r \in \widetilde{W}_{h,\Lambda}. \tag{74c}$$

Substituting $\boldsymbol{v} = \tilde{\boldsymbol{e}}^{\boldsymbol{u}}_{h,\Lambda}$, $q = \tilde{e}^{p}_{h,\Lambda}$ and $r = \tilde{e}^{\tilde{p}}_{h,\Lambda}$ into (74) and bounding the terms separately leads to

$$|\tilde{\boldsymbol{e}}^{\boldsymbol{u}}_{h,\Lambda}|^2_{\bar{a}_0} \leq \Big(E_{\max}\,|\boldsymbol{u}_{h^*,\Lambda} - \boldsymbol{u}_{h,\Lambda}|_{\bar{a}_0} + \sqrt{d}\,|p_{h^*,\Lambda} - p_{h,\Lambda}|_{\bar{c}}\Big)\,|\tilde{\boldsymbol{e}}^{\boldsymbol{u}}_{h,\Lambda}|_{\bar{a}_0}, \tag{75a}$$

$$|\tilde{e}^{p}_{h,\Lambda}|^2_{\bar{c}} \leq \Big(\sqrt{d}\,|\boldsymbol{u}_{h^*,\Lambda} - \boldsymbol{u}_{h,\Lambda}|_{\bar{a}_0} + |\tilde{p}_{h^*,\Lambda} - \tilde{p}_{h,\Lambda}|_{\bar{d}_0}\Big)\,|\tilde{e}^{p}_{h,\Lambda}|_{\bar{c}}, \tag{75b}$$

$$|\tilde{e}^{\tilde{p}}_{h,\Lambda}|^2_{\bar{d}_0} \leq \Big(|p_{h^*,\Lambda} - p_{h,\Lambda}|_{\bar{c}} + E_{\max}\,|\tilde{p}_{h^*,\Lambda} - \tilde{p}_{h,\Lambda}|_{\bar{d}_0}\Big)\,|\tilde{e}^{\tilde{p}}_{h,\Lambda}|_{\bar{d}_0}. \tag{75c}$$

Combining all three estimates in (75) leads to the left-hand inequality in (71).

In order to prove the right-hand inequality in (71), we need to use a discrete stability result which is analogous to the one given in Lemma 3.1. Since $\mathcal{U}_{h^*,\Lambda} - \mathcal{U}_{h,\Lambda} \in \boldsymbol{V}_{h^*,\Lambda} \times W_{h^*,\Lambda} \times W_{h^*,\Lambda}$, there exists $\mathcal{V} := (\boldsymbol{v}, q, r) \in \boldsymbol{V}_{h^*,\Lambda} \times W_{h^*,\Lambda} \times W_{h^*,\Lambda}$ with

$$|||\mathcal{V}|||=\big(|\boldsymbol{v}|^2_{\bar{a}_0} + |q|^2_{\bar{c}} + |r|^2_{\bar{d}_0}\big)^{1/2} \leq \widehat{C}_2\,|||\mathcal{U}_{h^*,\Lambda} - \mathcal{U}_{h,\Lambda}||| \tag{76}$$

satisfying

$$E_{\min}\,\widehat{C}_1\,|||\mathcal{U}_{h^*,\Lambda} - \mathcal{U}_{h,\Lambda}|||^2 \leq \mathcal{B}(\mathcal{U}_{h^*,\Lambda} - \mathcal{U}_{h,\Lambda}; \mathcal{V}), \tag{77}$$

where $\widehat{C}_1$ and $\widehat{C}_2$ are defined analogously to the constants C_1^* and C_2^* in Lemma 3.1 but with γ_h replaced by the inf–sup constant γ_h^* associated with the spaces $\boldsymbol{V}_h^*$ and W_h^*. Recalling the definitions of $\boldsymbol{V}_{h^*,\Lambda}$ and $W_{h^*,\Lambda}$ and the associated decompositions in (28) and (29), we may decompose $\mathcal{V} \in \boldsymbol{V}_{h^*,\Lambda} \times W_{h^*,\Lambda} \times W_{h^*,\Lambda}$ as $\mathcal{V} = \mathcal{V}_{h,\Lambda} + \widetilde{\mathcal{V}}_{h,\Lambda}$, where $\mathcal{V}_{h,\Lambda} := (\boldsymbol{v}_{h,\Lambda}, q_{h,\Lambda}, r_{h,\Lambda}) \in \boldsymbol{V}_{h,\Lambda} \times W_{h,\Lambda} \times W_{h,\Lambda}$ and $\widetilde{\mathcal{V}}_{h,\Lambda} := (\tilde{\boldsymbol{v}}_{h,\Lambda}, \tilde{q}_{h,\Lambda}, \tilde{r}_{h,\Lambda}) \in \widetilde{\boldsymbol{V}}_{h,\Lambda} \times \widetilde{W}_{h,\Lambda} \times \widetilde{W}_{h,\Lambda}$. Since $\mathcal{B}(\mathcal{U}_{h^*,\Lambda} - \mathcal{U}_{h,\Lambda}; \mathcal{V}_{h,\Lambda}) = 0$, we use equations (74) and the Cauchy–Schwarz inequality to give

$$\begin{aligned} E_{\min}\,\widehat{C}_1\,|||\mathcal{U}_{h^*,\Lambda} - \mathcal{U}_{h,\Lambda}|||^2 &\leq \mathcal{B}(\mathcal{U}_{h^*,\Lambda} - \mathcal{U}_{h,\Lambda}; \widetilde{\mathcal{V}}_{h,\Lambda}) \\ &\overset{(74)}{=} \bar{a}_0(\tilde{\boldsymbol{e}}^{\boldsymbol{u}}_{h,\Lambda}, \tilde{\boldsymbol{v}}_{h,\Lambda}) + \bar{c}(\tilde{e}^{p}_{h,\Lambda}, \tilde{q}_{h,\Lambda}) + \bar{d}_0(\tilde{e}^{\tilde{p}}_{h,\Lambda}, \tilde{r}_{h,\Lambda}) \\ &\leq |\tilde{\boldsymbol{e}}^{\boldsymbol{u}}_{h,\Lambda}|_{\bar{a}_0}|\tilde{\boldsymbol{v}}_{h,\Lambda}|_{\bar{a}_0} + |\tilde{e}^{p}_{h,\Lambda}|_{\bar{c}}|\tilde{q}_{h,\Lambda}|_{\bar{c}} + |\tilde{e}^{\tilde{p}}_{h,\Lambda}|_{\bar{d}_0}|\tilde{r}_{h,\Lambda}|_{\bar{d}_0}. \end{aligned} \tag{78}$$

We will now estimate $|\tilde{\boldsymbol{v}}_{h,\Lambda}|_{\bar{a}_0}$, $|\tilde{q}_{h,\Lambda}|_{\bar{c}}$, and $|\tilde{r}_{h,\Lambda}|_{\bar{d}_0}$. Using the strengthened Cauchy–Schwarz inequality in (26a), we have

$$\begin{aligned} |\tilde{\boldsymbol{v}}_{h,\Lambda}|^2_{\bar{a}_0} &= |\boldsymbol{v}|^2_{\bar{a}_0} - 2\bar{a}_0(\boldsymbol{v}_{h,\Lambda}, \tilde{\boldsymbol{v}}_{h,\Lambda}) - |\boldsymbol{v}_{h,\Lambda}|^2_{\bar{a}_0} \leq |\boldsymbol{v}|^2_{\bar{a}_0} + 2\gamma_1|\boldsymbol{v}_{h,\Lambda}|_{\bar{a}_0}|\tilde{\boldsymbol{v}}_{h,\Lambda}|_{\bar{a}_0} - |\boldsymbol{v}_{h,\Lambda}|^2_{\bar{a}_0} \\ &\leq |\boldsymbol{v}|^2_{\bar{a}_0} + |\boldsymbol{v}_{h,\Lambda}|^2_{\bar{a}_0} + \gamma_1^2|\tilde{\boldsymbol{v}}_{h,\Lambda}|^2_{\bar{a}_0} - |\boldsymbol{v}_{h,\Lambda}|^2_{\bar{a}_0} = |\boldsymbol{v}|^2_{\bar{a}_0} + \gamma_1^2|\tilde{\boldsymbol{v}}_{h,\Lambda}|^2_{\bar{a}_0}, \end{aligned}$$

which yields

$$|\tilde{\boldsymbol{v}}_{h,\Lambda}|_{\bar{a}_0} \leq (1 - \gamma_1^2)^{-1/2}|\boldsymbol{v}|_{\bar{a}_0}. \tag{79a}$$

In the same way, using (26b), we obtain

$$|\tilde{q}_{h,\Lambda}|_{\bar{c}} \leq (1 - \gamma_2^2)^{-1/2}|q|_{\bar{c}}, \qquad |\tilde{r}_{h,\Lambda}|_{\bar{d}_0} \leq (1 - \gamma_2^2)^{-1/2}|r|_{\bar{d}_0}. \tag{79b}$$

Combining (78) and (79), using (76) and recalling the definition of $\eta_{h^*,\Lambda}$ in (70a), establishes the right-hand inequality in (71) with $\gamma = \max\{\gamma_1, \gamma_2\}$. □

Instead of computing the projection of the error by solving problem (69), we could have simply used $|e_0^p|_{\bar{c}}$ directly in the definition (70) of $\eta_{h^*,\Lambda}$. This would lead to a small saving in the computational overhead. The reason we did not do this is the fact that a saturation constant would then need to be included in order to establish the upper bound corresponding to (71).

6. Balanced error reduction using adaptive refinement

Following convention, our adaptive strategy is to solve the SG-MFEM problem (22) and estimate the energy error. The approximation is then refined by adaptively enriching the underlying approximation spaces, until $\eta < \texttt{tol}$, where $\texttt{tol}$ is a user-prescribed tolerance. What is distinctive about our proposed refinement strategy is the separation of the component contributions of the spatial error from individual contributions of the parametric error.

6.1. The parametric error estimators.

We discuss the key features of the *parametric* error estimators $\boldsymbol{e}^{\boldsymbol{u}}_{h,\mathfrak{Q}}$ and $e^{\tilde{p}}_{h,\mathfrak{Q}}$ in this section. Recall that these contribute to η_1 and η_3 and hence the total error estimate η as well as the error reduction proxy $\eta_{h,\mathfrak{Q}}$. Let $\mathfrak{Q}$ be any finite detail index set, i.e., let $\mathfrak{Q}\subset\{\boldsymbol{\alpha}\in\mathfrak{I};\ \boldsymbol{\alpha}\notin\Lambda\}$. Since the subspaces $\boldsymbol{V}_h\otimes\operatorname{span}\{\psi_{\boldsymbol{\alpha}}\}$ with $\boldsymbol{\alpha}\in\mathfrak{Q}$ are pairwise orthogonal with respect to the inner product $\bar{a}_0(\cdot,\cdot)$, the parametric error estimator $\boldsymbol{e}^{\boldsymbol{u}}_{h,\mathfrak{Q}}$ defined in (60a) can be decomposed into separate contributions associated with the individual multi-indices $\boldsymbol{\alpha}\in\mathfrak{Q}$ as follows:

$$\boldsymbol{e}^{\boldsymbol{u}}_{h,\mathfrak{Q}} = \sum_{\boldsymbol{\alpha}\in\mathfrak{Q}} \boldsymbol{e}^{\boldsymbol{u}}_{h,\boldsymbol{\alpha}} \quad\text{with}\quad |\boldsymbol{e}^{\boldsymbol{u}}_{h,\mathfrak{Q}}|^2_{\bar{a}_0} = \sum_{\boldsymbol{\alpha}\in\mathfrak{Q}} |\boldsymbol{e}^{\boldsymbol{u}}_{h,\boldsymbol{\alpha}}|^2_{\bar{a}_0}, \tag{80}$$

where, for each $\boldsymbol{\alpha}\in\mathfrak{Q}$, the estimator $\boldsymbol{e}^{\boldsymbol{u}}_{h,\boldsymbol{\alpha}}\in\boldsymbol{V}_h\otimes\operatorname{span}\{\psi_{\boldsymbol{\alpha}}\}$ satisfies

$$\bar{a}_0(\boldsymbol{e}^{\boldsymbol{u}}_{h,\boldsymbol{\alpha}},\boldsymbol{v}_h\psi_{\boldsymbol{\alpha}}) = \mathcal{R}^{\boldsymbol{u}}(\boldsymbol{v}_h\psi_{\boldsymbol{\alpha}}) \quad \forall\,\boldsymbol{v}_h\in\boldsymbol{V}_h. \tag{81}$$

Hence to compute $|\boldsymbol{e}^{\boldsymbol{u}}_{h,\mathfrak{Q}}|^2_{\bar{a}_0}$ we simply solve a set of decoupled Poisson problems associated with the finite element space $\boldsymbol{V}_h$. A similar decomposition holds for the parametric error estimator $e^{\tilde{p}}_{h,\mathfrak{Q}}$ defined in (60b) and we will denote the individual estimators associated with each multi-index $\boldsymbol{\alpha}\in\mathfrak{Q}$ by $e^{\tilde{p}}_{h,\boldsymbol{\alpha}}\in W_h\otimes\operatorname{span}\{\psi_{\boldsymbol{\alpha}}\}$. Next, thanks to Theorem 5.1, we see that the quantity $\eta_{h,\boldsymbol{\alpha}} := \big(|\boldsymbol{e}^{\boldsymbol{u}}_{h,\boldsymbol{\alpha}}|^2_{\bar{a}_0} + |e^{\tilde{p}}_{h,\boldsymbol{\alpha}}|^2_{\bar{a}_0}\big)^{1/2}$ (cf. (70b)) can be used to estimate the error reduction that would be achieved by adding only *one* multi-index $\boldsymbol{\alpha}\in\mathfrak{I}\setminus\Lambda$ to the current index set Λ and computing the corresponding enhanced approximation $\mathcal{U}_{h,\Lambda^*}$ with $\Lambda^*=\Lambda\cup\{\boldsymbol{\alpha}\}$.

An important aspect of our error estimation strategy (and a key ingredient of the adaptive algorithm presented below) is the choice of the detail index set $\mathfrak{Q}$. Let $\boldsymbol{t}^{(n)} = (t^{(n)}_1, t^{(n)}_2,\ldots)\in\mathfrak{I}$ be the Kronecker delta index for the coordinate $n\in\mathbb{N}$, i.e., $t^{(n)}_j=\delta_{jn}$ for any $j\in\mathbb{N}$. Next, for any finite index set Λ, we define Λ^*_∞ as the infinite index set given by $\Lambda^*_\infty = \Lambda\cup\mathfrak{Q}_\infty$, where

$$\mathfrak{Q}_\infty := \{\boldsymbol{\alpha}\in\mathfrak{I}\setminus\Lambda;\ \boldsymbol{\alpha}=\boldsymbol{\tau}\pm\boldsymbol{t}^{(n)} \text{ for some } \boldsymbol{\tau}\in\Lambda \text{ and some } n>0\} \tag{82}$$

denotes the boundary of Λ. The following result follows immediately from Corollary 4.1 in [6].

Lemma 6.1. *Suppose that $\mathfrak{Q}$ is a finite subset of the index set $\mathfrak{I}\setminus\Lambda^*_\infty$. Then the parametric error estimators $\boldsymbol{e}^{\boldsymbol{u}}_{h,\mathfrak{Q}}$ and $e^{\tilde{p}}_{h,\mathfrak{Q}}$ are identically equal to zero.*

Hence, nonzero contributions to $\boldsymbol{e}^{\boldsymbol{u}}_{h,\mathfrak{Q}}$ and $e^{\tilde{p}}_{h,\mathfrak{Q}}$ are associated only with the indices from the boundary index set $\mathfrak{Q}_\infty$. This has two consequences. First, for the error estimation to be effective, $\mathfrak{Q}$ should be chosen as a sufficiently large (finite) subset of $\mathfrak{Q}_\infty$. Second, for the adaptive algorithm to be efficient, the index set Λ should only be enriched at each step with multi-indices from the index set $\mathfrak{Q}_\infty$.

6.2. **An adaptive algorithm.** Let us first focus on the computation of $\eta = (\eta_1 + \eta_2 + \eta_3)^{1/2}$, where η_1, η_2, η_3 are defined in (57). Recall that η_2 is calculated directly using (49). To compute the spatial and parametric error estimators that contribute to η_1, η_3 (see (61), (62)), one needs to specify the detail finite element spaces $\widetilde{\boldsymbol{V}}_h$, $\widetilde{W}_h$ and the detail polynomial space $S_{\mathfrak{Q}}$ on the parameter domain Γ. Working in our IFISS software environment [14], [28], $\widetilde{\boldsymbol{V}}_h$ and $\widetilde{W}_h$ will span local bubble functions, for which we have two alternatives: (option I) piecewise polynomials of the same order as $\boldsymbol{V}_h$ and W_h, respectively on a uniformly refined mesh $\mathcal{T}_{h/2}$; and (option II) piecewise polynomials of a higher order on the mesh $\mathcal{T}_h$. In both cases, the computation of the spatial estimators $\tilde{\boldsymbol{e}}^{\boldsymbol{u}}_{h,\Lambda}$ and $\tilde{e}^{\tilde{p}}_{h,\Lambda}$ is broken down over the elements $K \in \mathcal{T}_h$ using the standard element residual technique (see, e.g., [1]).

The construction of the detail index set $\mathfrak{Q}$ (that defines $S_{\mathfrak{Q}}$) is motivated by Lemma 6.1. Specifically, we will use the following finite subset of the index set $\mathfrak{Q}_\infty$ defined in (82):

(83)
$$\mathfrak{Q} := \{\boldsymbol{\alpha} \in \mathfrak{I} \setminus \Lambda;\ \boldsymbol{\alpha} = \boldsymbol{\tau} \pm \boldsymbol{t}^{(n)} \text{ for some } \boldsymbol{\tau} \in \Lambda \text{ and some } n = 1, \ldots, M_\Lambda + 1\},$$

where $M_\Lambda \in \mathbb{N}$ (the number of active parameters) is defined as

$$M_\Lambda := \begin{cases} 0 & \text{if } \Lambda = \{(0,0,\ldots)\}, \\ \max\big\{\max(\operatorname{supp}(\boldsymbol{\alpha}));\ \boldsymbol{\alpha} \in \Lambda \setminus \{(0,0,\ldots)\}\big\} & \text{otherwise.} \end{cases}$$

Given the index set $\mathfrak{Q}$ in (83), the parametric error estimators $\boldsymbol{e}^{\boldsymbol{u}}_{h,\mathfrak{Q}}$ and $e^{\tilde{p}}_{h,\mathfrak{Q}}$ contributing to η_1, η_3 are computed from the corresponding individual error estimators $\boldsymbol{e}^{\boldsymbol{u}}_{h,\boldsymbol{\alpha}}$ and $e^{\tilde{p}}_{h,\boldsymbol{\alpha}}$ for each $\boldsymbol{\alpha} \in \mathfrak{Q}$ as explained in Section 6.1 (see, e.g., (80)–(81)).

Let us now describe the refinement procedure. The emphasis is on simplicity. If the estimated error η is too large then, in order to compute a more accurate approximation, one needs to enrich the finite-dimensional subspaces $\boldsymbol{V}_{h,\Lambda} = \boldsymbol{V}_h \otimes S_\Lambda$ and $W_{h,\Lambda} = W_h \otimes S_\Lambda$. Recall that the quantities (see (70))

$$\eta_{h^*,\Lambda} = \big(|\tilde{\boldsymbol{e}}^{\boldsymbol{u}}_{h,\Lambda}|^2_{\tilde{a}_0} + |\tilde{e}^{p}_{h,\Lambda}|^2_{\tilde{c}} + |\tilde{e}^{\tilde{p}}_{h,\Lambda}|^2_{\tilde{d}_0}\big)^{1/2} \quad \text{and} \quad \eta_{h,\boldsymbol{\alpha}} = \big(|\boldsymbol{e}^{\boldsymbol{u}}_{h,\boldsymbol{\alpha}}|^2_{\tilde{a}_0} + |e^{\tilde{p}}_{h,\boldsymbol{\alpha}}|^2_{\tilde{d}_0}\big)^{1/2} \tag{84}$$

(for $\boldsymbol{\alpha} \in \mathfrak{Q}$) provide proxies for the potential error reductions associated with spatial and parametric enrichment, respectively (in the latter case, the enrichment is associated with adding a single index $\boldsymbol{\alpha} \in \mathfrak{Q}$); see Theorem 5.1. We use the dominant proxy to guide the enrichment of $\boldsymbol{V}_{h,\Lambda}$ and $W_{h,\Lambda}$. More precisely, if $\eta_{h^*,\Lambda} \geq \tau\, \eta_{h,\mathfrak{Q}}$ with a refinement weighting factor $\tau \geq 1$, then the finite element spaces $\boldsymbol{V}_h$ and W_h are enriched by refining the finite element mesh on D; otherwise, the polynomial space S_Λ on Γ is enriched by adding at least one new index to the set Λ. In the latter case, we enrich Λ with indices $\boldsymbol{\alpha}$ that are generated from a (Dörfler) bulk marking procedure. This builds a subset of indices $\mu(\mathfrak{Q})$ of minimum cardinality such that $\sum_{\boldsymbol{\alpha}_i \in \mu(\mathfrak{Q})} \eta^2_{h,i} \geq \theta \eta^2_{h,\mathfrak{Q}}$ with marking parameter $\theta = 1/2$.

Our adaptive strategy is presented in Algorithm 6.1. Starting with an inf–sup stable pair $\boldsymbol{V}_{h_0}$–W_{h_0} of finite element spaces on a coarse mesh $\mathcal{T}_{h_0}$ and with an initial index set Λ_0 (typically, $\Lambda = \{(0,0,0,\ldots)\}$ or $\Lambda = \{(0,0,0,\ldots),\ (1,0,0,\ldots)\}$), the algorithm generates two sequences of finite element spaces

$$\boldsymbol{V}_{h_0} \subseteq \boldsymbol{V}_{h_1} \subseteq \ldots \subseteq \boldsymbol{V}_{h_K} \subset \boldsymbol{H}^1_{E_0}(D) \quad \text{and} \quad W_{h_0} \subseteq W_{h_1} \subseteq \ldots \subseteq W_{h_K} \subset L^2(D),$$

a sequence of index sets $\Lambda_0 \subseteq \Lambda_1 \subseteq \Lambda_2 \ldots \subseteq \Lambda_K \subset \mathfrak{I}$, as well as a sequence of SG-MFEM approximations $(\boldsymbol{u}_k, p_k, \tilde{p}_k) \in \boldsymbol{V}_{h_k,\Lambda_k} \times W_{h_k,\Lambda_k} \times W_{h_k,\Lambda_k}$ and the corresponding error estimates $\eta^{(k)}$ $(k=0,1,\ldots,K)$. The refinement weighting factor is chosen to be $\tau = \sqrt{2}$, and the algorithm is terminated when the estimated error is sufficiently small.

Algorithm 6.1. `Adaptive_SG-MFEM` $\big[\mathtt{tol}, \mathcal{B}, f, h_0, \Lambda_0\big] \to \big[(\boldsymbol{u}_K, p_K, \tilde{p}_K), \eta^{(K)}\big]$
for $k = 0, 1, 2, \ldots$ **do**
$(\boldsymbol{u}_k, p_k, \tilde{p}_k) \leftarrow \mathtt{Solve}\big[\mathcal{B}, f, \boldsymbol{V}_{h_k}, W_{h_k}, \Lambda_k\big]$
$[\delta_h, \eta_{h^*,\Lambda}] \leftarrow \mathtt{Error\_Estimate\_1}\big[\mathcal{B}, f, \boldsymbol{u}_k, p_k, \tilde{p}_k, \widetilde{\boldsymbol{V}}_{h_k}, \widetilde{W}_{h_k}\big]$
$\mathfrak{Q}_k \leftarrow \mathtt{Detail\_Index\_Set}\big[\Lambda_k\big]$
for $i = 1, 2, \ldots, \#(\mathfrak{Q}_k)$ **do**
$\eta_{h,i} \leftarrow \mathtt{Error\_Estimate\_2}\big[\mathcal{B}, f, \boldsymbol{u}_k, p_k, \tilde{p}_k, \boldsymbol{\alpha}_i\big]$
end
$\eta_{h,\mathfrak{Q}} := \Big(\sum_{i=1}^{\#(\mathfrak{Q}_k)} \eta_{h,i}^2\Big)^{1/2}$
$\eta^{(k)} := \big(\delta_h^2 + \eta_{h,\mathfrak{Q}}^2\big)^{1/2}$
if $\eta^{(k)} < \mathtt{tol}$ **then** $K := k$**, break**
if $\eta_{h^*,\Lambda} \geq \sqrt{2}\,\eta_{h,\mathfrak{Q}}$ **then**
$\boldsymbol{V}_{h_{k+1}} := \boldsymbol{V}_{h_k^*}$, $W_{h_{k+1}} := W_{h_k^*}$, $\Lambda_{k+1} := \Lambda_k$
else $\boldsymbol{V}_{h_{k+1}} := \boldsymbol{V}_{h_k}$, $W_{h_{k+1}} := W_{h_k}$, $\Lambda_{k+1} := \Lambda_k \cup \big\{\boldsymbol{\alpha}_i \in \mu(\mathfrak{Q}_k)\big\}$
end

The algorithm has four functional building blocks:

- `Solve`$\big[\mathcal{B}, f, \boldsymbol{V}_h, W_h, \Lambda\big]$: a subroutine that generates the SG-MFEM approximation $(\boldsymbol{u}_{h,\Lambda}, p_{h,\Lambda}, \tilde{p}_{h,\Lambda}) \in \boldsymbol{V}_{h,\Lambda} \times W_{h,\Lambda} \times W_{h,\Lambda}$ satisfying (22);
- `Detail_Index_Set`$\big[\Lambda\big]$: a subroutine that generates the detail index set $\mathfrak{Q}$ for the given index set Λ (see (83));
- `Error_Estimate_1` $\big[\mathcal{B}, f, \boldsymbol{u}_{h,\Lambda}, p_{h,\Lambda}, \tilde{p}_{h,\Lambda}, \widetilde{\boldsymbol{V}}_h, \widetilde{W}_h\big]$: a subroutine that computes $\delta_h := (|\tilde{\boldsymbol{e}}^{\boldsymbol{u}}_{h,\Lambda}|^2_{\bar{a}_0} + |e_0^p|^2_{\bar{c}} + |\tilde{e}^{\tilde{p}}_{h,\Lambda}|^2_{\bar{d}_0})^{1/2}$, the contribution to η associated with spatial enrichment, and the spatial error reduction proxy $\eta_{h^*,\Lambda}$ in (84);
- `Error_Estimate_2` $\big[\mathcal{B}, f, \boldsymbol{u}_{h,\Lambda}, p_{h,\Lambda}, \tilde{p}_{h,\Lambda}, \boldsymbol{\alpha}\big]$: a subroutine that computes the parametric error reduction proxy associated with a single index $\boldsymbol{\alpha} \in \mathfrak{Q}$ (see (84)).

The IFISS software environment that we use to test the efficiency of our methodology is limited to two-dimensional spatial approximation. It provides two alternative choices for the *spatial refinement* step in Algorithm 6.1 that is taken whenever the spatial refinement proxy $\eta_{h^*,\Lambda}$ dominates the parametric refinement proxy $\eta_{h,\mathfrak{Q}}$. In cases where the solution is spatially smooth, a natural option is to define h_k^* by taking a *uniform* refinement of the current grid. In the computational experiments discussed later, this refinement option is associated with a rectangular subdivision of the spatial domain.[2] On the other hand, when solving spatially singular problems, it is more natural to define h_k^* by a *local* refinement strategy in combination

[2]Specifically, we always use uniform refinement in combination with the inf–sup stable approximation pairs that are built into the S-IFISS toolbox [29].

with triangular approximation. In our T-IFISS toolbox implementation [28] this is done using a standard iterative refinement loop

$$\text{Solve} \rightarrow \text{Estimate} \rightarrow \text{Mark} \rightarrow \text{Refine}$$

combined with a bulk parameter marking procedure with the same marking parameter $\theta = 1/2$ as used for the parametric enrichment. The local mesh refinement is performed using a longest edge bisection strategy, which is a variant of the newest vertex bisection (NVB) method. Further details are given in [4].

The attractive feature of NVB refinement strategies is that they lead to nested finite element spaces [25, p.179]. This is a key ingredient in the proof of the contraction property for adaptive finite element approximations. A comprehensive numerical study of the alternative refinement and marking strategies that are built into T-IFISS can be found in [5]. The sparse (Galerkin) high-dimensional system of linear equations that is generated at each step of the adaptive algorithm is solved using a bespoke MINRES solver (EST_MINRES) in combination with the efficient preconditioning strategy presented in [22].

7. Computational results

In this section, we present two numerical examples that support the theoretical results. In the first experiment, we consider a simple test problem with an exact solution and investigate the accuracy of the a posteriori error estimate η. In the second, we consider a problem where the Young modulus depends on a countably infinite set of parameters and illustrate the effectiveness of the adaptive algorithm.

7.1. **Exact solution, Dirichlet boundary condition.** To define a problem of the form (2) with an exact solution, we choose the spatial domain $D = (0,1)^2$ and impose a Dirichlet condition on the displacement $\boldsymbol{u}$ on the whole boundary. Hence, $\partial D_D = \partial D$ and $\partial D_N = \emptyset$. (Thus the discretised problem is singular when $\nu = 1/2$. This does not impinge on the convergence of the iterative solver for the values of ν that we consider.) The uncertain Young modulus is modelled as $E := e_0 + 0.1y_1$ where $y_1 \in [-1,1]$ is the image of a mean zero uniform random variable. Hence, E is spatially constant and $e_0 = 1$ is the mean. The body force

$$\boldsymbol{f} = \begin{cases} f_1 = -2\alpha\pi^3 \cos(\pi x_2)\sin(\pi x_2)(2\cos(2\pi x_1) - 1), \\ f_2 = 2\alpha\pi^3 \cos(\pi x_1)\sin(\pi x_1)(2\cos(2\pi x_2) - 1), \end{cases} \tag{85}$$

is chosen so that the exact displacement is

$$\boldsymbol{u} = \begin{cases} u_1 = \pi \cos(\pi x_2)\sin(\pi x_2)\sin^2(\pi x_1)/E, \\ u_2 = -\pi \cos(\pi x_1)\sin(\pi x_1)\sin^2(\pi x_2)/E, \end{cases} \tag{86}$$

and the exact pressure is $p = \tilde{p} = 0$. For the spatial discretisation we use $\boldsymbol{Q}_2$–P_{-1}–P_{-1} approximation on uniform grids of square elements.[3] To compute the SG-MFEM solution, we choose S_Λ to be the space of polynomials of degree less than or equal to k in y_1 on $\Gamma = [-1,1]$. To assess the quality of the error estimate we will examine

$$\text{Effectivity index} := \frac{\eta}{\mathcal{E}},$$

[3]The combination $\boldsymbol{Q}_2$–P_{-1} is one of the most effective inf–sup stable approximation pairs in a two-dimensional uniform refinement setting; see [15, Sect. 3.3.1].

where $\mathcal{E}$ is the error defined in Corollary 4.5, as we vary the SG-MFEM discretisation parameters h and k. Results for five representative values of the Poisson ratio ν are presented in Tables 1 and 2. To compute the error estimate η, we consider two types of finite element detail spaces based on local bubble functions (option I, option II), as explained in Section 6.2. Since we have only one parameter y_1, the polynomial space S_Ω is chosen to be the set of polynomials of degree equal to $k+1$.

TABLE 1. Test problem 1: Effectivity indices for fixed polynomial degree $k = 3$ with two different types of hierarchical basis functions.

h	$\nu = .4$	$\nu = .49$	$\nu = .499$	$\nu = .4999$	$\nu = .49999$
option I					
2^{-3}	0.8992	0.9361	0.9405	0.9409	0.9409
2^{-4}	0.9196	0.9580	0.9625	0.9630	0.9630
2^{-5}	0.9251	0.9639	0.9684	0.9689	0.9690
2^{-6}	0.9267	0.9656	0.9701	0.9706	0.9706
option II					
2^{-3}	1.3311	1.3561	1.3591	1.3594	1.3594
2^{-4}	1.3435	1.3701	1.3732	1.3735	1.3736
2^{-5}	1.3468	1.3737	1.3769	1.3773	1.3773
2^{-6}	1.3477	1.3748	1.3780	1.3783	1.3783

The results confirm that our a posteriori error estimate is robust with respect to the Poisson ratio (in the incompressible limit), the finite element mesh size h and the polynomial degree k associated with the parametric approximation.

TABLE 2. Test problem 1: Effectivity indices for fixed finite element mesh size $h = 2^{-6}$ with two different types of hierarchical basis functions.

k	$\nu = .4$	$\nu = .49$	$\nu = .499$	$\nu = .4999$	$\nu = .49999$
option I					
2	0.9923	1.0287	1.0330	1.0334	1.0335
3	0.9266	0.9656	0.9701	0.9706	0.9706
4	0.9265	0.9654	0.9700	0.9704	0.9705
5	0.9265	0.9654	0.9700	0.9704	0.9705
option II					
2	1.3937	1.4198	1.4229	1.4233	1.4233
3	1.3477	1.3748	1.3780	1.3783	1.3783
4	1.3476	1.3747	1.3779	1.3782	1.3782
5	1.3476	1.3747	1.3779	1.3782	1.3782

7.2. **Singular problem, mixed boundary conditions.** To test our error estimation strategy in a more realistic setting we next consider a problem with a mixed boundary condition (so that $\partial D_N \neq \emptyset$). Specifically, we take the unit square domain with a homogeneous Neumann boundary condition on the right

edge $\partial D_N = \{1\} \times (0,1)$ and a zero Dirichlet boundary condition for the displacement on $\partial D_D = \partial D \setminus \partial D_N$. The uncertain Young modulus has mean value one and is given by the representation[4]

$$E(\boldsymbol{x},\boldsymbol{y}) = 1 + \sum_{m=1}^{\infty} \alpha_m \cos(2\pi\beta_1(m)x_1)\cos(2\pi\beta_2(m)x_2)y_m, \quad \boldsymbol{x} \in D, \boldsymbol{y} \in \Gamma, \tag{87}$$

where $\Gamma = \Pi_{m=1}^{\infty}\Gamma_m$ and $y_m \in \Gamma_m := [-1,1]$. For each $m \in \mathbb{N}$,

$$\beta_1(m) = m - k(m)(k(m)+1)/2 \quad \text{and} \quad \beta_2(m) = k(m) - \beta_1(m) \tag{88}$$

where $k(m) = -1/2 + \sqrt{1/4 + 2m}$ and $\alpha_m = \bar{\alpha} m^{-\tilde{\sigma}}$ for fixed $\tilde{\sigma} > 1$ and $0 < \bar{\alpha} < 1/\zeta(\tilde{\sigma})$, where ζ is the Riemann zeta function.

We present results for the case of a horizontal body force $\boldsymbol{f} = (0.1, 0)^\top$. This generates an exact displacement solution that is symmetric about the line $y = 1/2$. The problem has limited regularity in the compressible case: for $\nu = 0.4$ there are strong singularities at the two corners where the boundary condition changes from essential to natural. The singularities become progressively weaker in the incompressible limit and their effect on the solution is imperceptible when $\nu = 0.49999$.

To ensure a reasonable level of accuracy in the singular cases we used $\boldsymbol{P}_2$–P_1–P_1 triangular approximation[5] in combination with spatial adaptivity. The number of displacement degrees of freedom in the initial mesh $\mathcal{T}_{h_0}$ was 162. The adaptive algorithm was terminated when the estimated error was reduced by two orders of magnitude. We checked the convergence of Algorithm 6.1 for two choices of coefficient α_m in (87): $\tilde{\sigma} = 2$ (slow decay) and $\tilde{\sigma} = 4$ (fast decay). Results for the slow decay case are shown in Figures 1–3.

We make the following observations.

- The rate of convergence is $O(n^{-1/2})$ (where n is the total number of degrees of freedom) and is independent of the Poisson ratio.
- The plateaus in the parametric error proxy $\eta_{h,\mathcal{Q}}$ correspond to spatial refinement steps. The error estimate η is initially dominated by the spatial error proxy $\eta_{h^*,\Lambda}$ in the compressible case, that is when $\nu = 0.4$. In contrast, the parametric error contribution dominates the initial steps of the adaptive algorithm in the nearly incompressible case.
- Looking at Figure 2 the number of adaptive steps taken to reach the error tolerance is very similar. We can also see that three times as many indices are activated in the nearly incompressible case.
- The number of displacement degrees of freedom in the mesh when the algorithm terminated was $95,004$ when $\nu = 0.4$ and $17,610$ in the nearly incompressible case. These meshes are shown in Figure 3 and clearly illustrate the influence of the spatial singularities in the compressible case.

Analogous results obtained in the fast decay case are shown in Figures 4–5. We make two final observations.

- Once again, the rate of convergence is $O(n^{-1/2})$ (where n is the total number of degrees of freedom) and is independent of the Poisson ratio.

[4]This parametric representation is commonly used in the literature (see, for example, [12]). It characterises one of several test problems that are built into the S-IFISS toolbox [29].

[5]The (Taylor–Hood) combination $\boldsymbol{P}_2$–P_1 is the best known inf–sup stable approximation pair; see [15, Sect. 3.3.3].

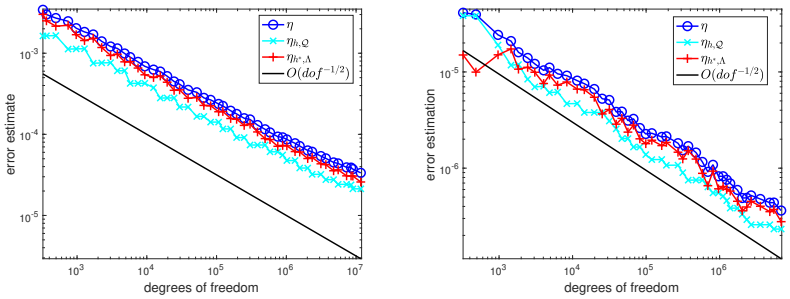

FIGURE 1. Test problem 2 (slow decay, $\tilde{\sigma} = 2$): Estimated error at each step of Algorithm 6.1 for $\nu = .4$ (left); $\nu = 0.49999$ (right).

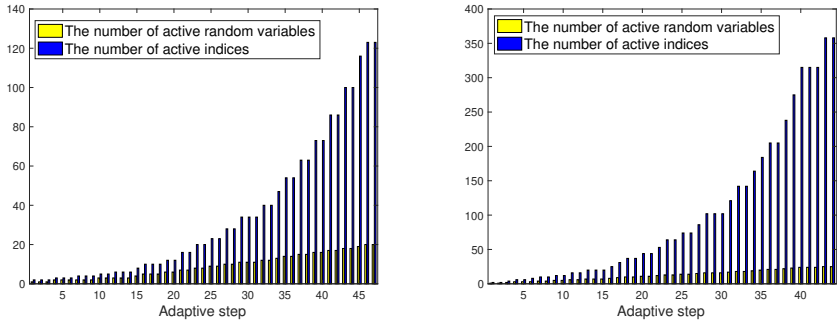

FIGURE 2. Test problem 2 (slow decay, $\tilde{\sigma} = 2$): The number of active multi-indices $\boldsymbol{\alpha}$ and active random variables y_m at each step of the Algorithm 6.1 for $\nu = .4$ (left); $\nu = 0.49999$ (right).

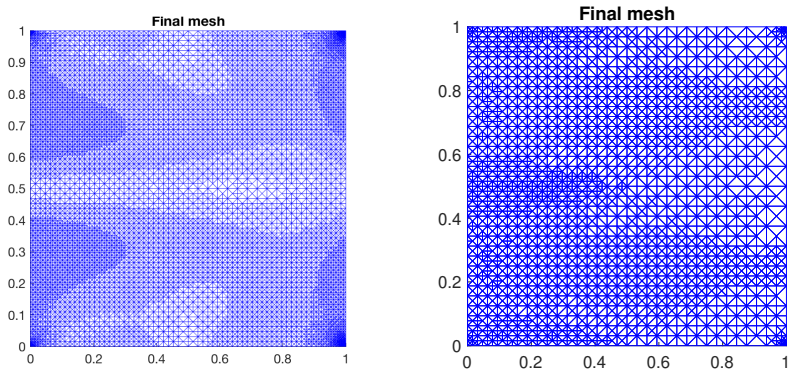

FIGURE 3. Test problem 2 (slow decay, $\tilde{\sigma} = 2$): triangular mesh at the step when the target number of degrees of freedom was reached for $\nu = .4$ (left); $\nu = 0.49999$ (right).

- Comparing Figure 2 with Figure 5 we see that the number of parameters (and indices) that are activated in the fast decay case is much less than the

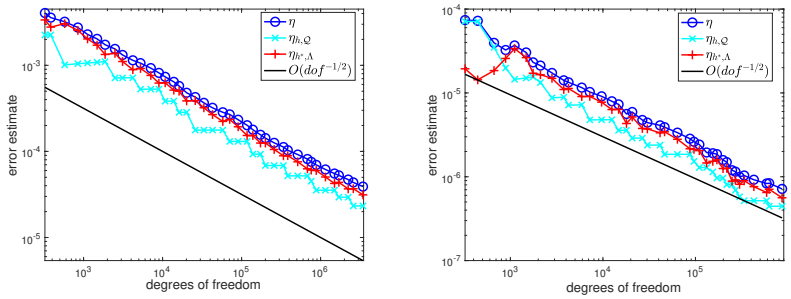

FIGURE 4. Test problem 2 (fast decay, $\tilde{\sigma} = 4$): Estimated error at each step of Algorithm 6.1 for $\nu = .4$ (left); $\nu = 0.49999$ (right).

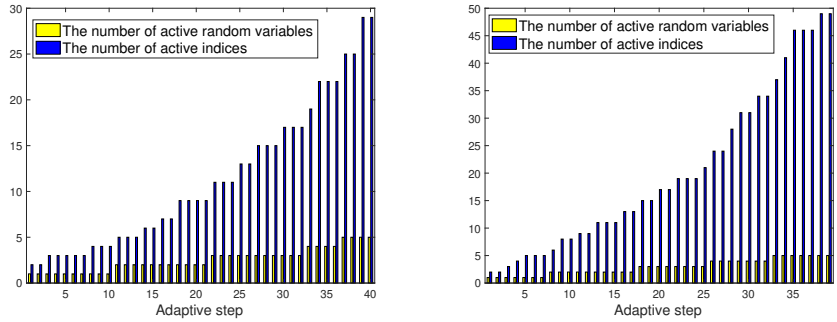

FIGURE 5. Test problem 2 (fast decay, $\tilde{\sigma} = 4$): The number of active multi-indices $\boldsymbol{\alpha}$ and active random variables y_m at each step of the Algorithm 6.1 for $\nu = .4$ (left); $\nu = 0.49999$ (right).

number that were activated in the slow decay case for a similar number of degrees of freedom.

8. SUMMARY

Efficient adaptive algorithms hold the key to effective computational solution of PDEs of elliptic type with uncertain material coefficients. This paper has two important contributions, building on earlier work for scalar diffusion problems. First, we have shown that mixed formulations of elasticity equations with parametric uncertainty can be solved in a black-box fashion within a Galerkin framework as long as (i) the inner-products associated with the evaluation of the functional residuals are suitably chosen and (ii) the detail spaces are chosen in a way that fully exploits the underlying orthogonality of the parametric basis functions. We believe that this development opens the door to practical engineering analysis of structures with uncertain material coefficients. Second, in contrast to other work in this area, which typically estimates a posteriori errors by taking norms of residuals, our approach can give accurate proxies of potential error reductions that would occur if different refinement strategies were pursued. Extensive numerical testing confirms that effectivity indices close to unity can be maintained throughout the refinement process if these proxies are used used to drive the adaptive algorithm.

References

1. Mark Ainsworth and J. Tinsley Oden, *A posteriori error estimation in finite element analysis*, Wiley, 2000.
2. Markus Bachmayr, Albert Cohen, Dinh Düng, and Christoph Schwab, *Fully discrete approximation of parametric and stochastic elliptic PDEs*, SIAM J. Numer. Anal. **55** (2017), 2151–2186.
3. Randolph B. Bank and R. Kent Smith, *A posteriori error estimates based on hierarchical bases*, SIAM J. Numer. Anal. **30** (1993), no. 4, 921–935.
4. A. Bespalov, L. Rocchi, and D. Silvester, *T–IFISS: a toolbox for adaptive FEM computation*, Comput. Math. Appl. (2020), https://doi.org/10.1016/j.camwa.2020.03.005.
5. Alex Bespalov and Leonardo Rocchi, *Efficient adaptive algorithms for elliptic PDEs with random data*, SIAM/ASA J. Uncertainty Quantification **6** (2018), no. 1, 243–272.
6. Alex Bespalov and David J. Silvester, *Efficient adaptive stochastic Galerkin methods for parametric operator equations*, SIAM J. Sci. Comput. **38** (2016), no. 4, A2118–A2140.
7. Alexey Bespalov, Catherine Powell, and David Silvester, *Energy norm a posteriori error estimation for parametric operator equations*, SIAM J. Sci. Comput. **36** (2014), A339–A363, http://dx.doi.org/10.1137/130916849.
8. Daniele Boffi and Rolf Stenberg, *A remark on finite element schemes for nearly incompressible elasticity*, Computers and Mathematics with Applications **74** (2017), 2047–2055, http://dx.doi.org/10.1016/j.camwa.2017.06.006.
9. Albert Cohen and Ronald DeVore, *Approximation of high-dimensional parametric PDEs*, Acta Numerica **24** (2015), 1–159.
10. Adam J. Crowder and Catherine E. Powell, *CBS constants and their role in error estimation for stochastic Galerkin finite element methods*, Journal of Scientific Computing **77** (2018), 1030–1054.
11. Adam J. Crowder, Catherine E. Powell, and Alex Bespalov, *Efficient adaptive multilevel stochastic Galerkin approximation using implicit a posteriori error estimation*, SIAM J. Sci. Comput. **41** (2019), A1681–A1705, https://doi.org/10.1137/18M1194420.
12. Martin Eigel, Claude Jeffrey Gittelson, Christoph Schwab, and Elmar Zander, *Adaptive stochastic Galerkin FEM*, Computer Methods in Applied Mechanics and Engineering **270** (2014), 247–269.
13. Victor Eijkhout and Panayot Vassilevski, *The role of the strengthened Cauchy-Buniakowskiĭ-Schwarz inequality in multilevel methods*, SIAM Review **33** (1991), no. 3, 405–419.
14. Howard Elman, Alison Ramage, and David Silvester, *IFISS: A computational laboratory for investigating incompressible flow problems*, SIAM Review **56** (2014), no. 2, 261–273, http://dx.doi.org/10.1137/120891393.
15. Howard Elman, David Silvester, and Andy Wathen, *Finite elements and fast iterative solvers: with applications in incompressible fluid dynamics*, Oxford University Press, Oxford, UK, 2014, Second Edition, xiv+400 pp. ISBN: 978-0-19-967880-8.
16. Roger G. Ghanem and Pol D. Spanos, *Stochastic finite elements: A spectral approach*, Dover Publications Inc., 2012.
17. Diane Guignard and Fabio Nobile, *A posteriori error estimation for the stochastic collocation finite element method*, SIAM J. Numer. Anal. **56** (2018), no. 5, 3121–3143.
18. Leonard R. Herrmann, *Elasticity equations for incompressible and nearly incompressible materials by a variational theorem*, AIAA J. **3** (1965), 1896–1900.
19. Viet Ha Hoang, Thanh Chung Nguyen, and Bingxing Xia, *Polynomial approximations of a class of stochastic multiscale elasticity problems*, Zeitschrift für angewandte Mathematik und Physik **67** (2016), 78.
20. Paul Houston, Dominik Schötzau, and Thomas P. Wihler, *An hp-adaptive mixed discontinuous Galerkin FEM for nearly incompressible linear elasticity*, Comput. Methods Appl. Mech. Engrg **195** (2006), 3224–3246.
21. Arbaz Khan, Catherine E. Powell, and David J. Silvester, *Robust a posteriori error estimators for mixed approximation of nearly incompressible elasticity*, Int. J. Numer. Methods Eng. **119** (2019), 18–37, https://doi.org/10.1002/nme.6040.
22. Arbaz Khan, Catherine E. Powell, and David J. Silvester, *Robust preconditioning for stochastic Galerkin formulations of parameter-dependent nearly incompressible elasticity equations*, SIAM J. Sci. Comput. **41** (2019), A402–A421, https://doi.org/10.1137/18M117385X.

23. Reijo Kouhia and Rolf Stenberg, *A linear nonconforming finite element method for nearly incompressible elasticity and Stokes flow*, Comput. Methods Appl. Mech. Engrg **124** (1995), no. 3, 195–212.
24. Hermann G. Matthies, Christoph Brenner, Christian Bucher, and C. Guedes Soares, *Uncertainties in probabilistic numerical analysis of structures and solid–stochastic finite elements*, Struct. Safety **19** (1997), 283–336.
25. Ricardo Nochetto and Andreas Veeser, *Primer of Adaptive Finite Element Methods*, Multiscale and Adaptivity: Modeling, Numerics and Applications, vol. 2040, Springer-Verlag Berlin Heidelberg, 2012, pp. 125–225.
26. Serge Prudhomme and J. Tinsley Oden, *On goal-oriented error estimation for elliptic problems: application to the control of pointwise errors*, Comput. Methods Appl. Mech. Engrg. **176** (1999), no. 1-4, 313–331.
27. Shang Shen and Gun Jin Yun, *Stochastic finite element with material uncertainties: implementation in a general purpose simulation program*, Finite Elements in Analysis and Design (2013), 65–78.
28. David J. Silvester, Alex Bespalov, Qifeng Liao, and Leonardo Rocchi, *Triangular IFISS (TIFISS) version 1.2.*, December 2018, `http://www.manchester.ac.uk/ifiss/tifiss`.
29. David J. Silvester, Alex Bespalov, and Catherine E. Powell, *Stochastic IFISS (S-IFISS) version 1.04*, June 2017, `http://www.manchester.ac.uk/ifiss/s-ifiss1.0.tar.gz`.
30. Bingxing Xia and Viet Ha Hoang, *Best N-term GPC approximations for a class of stochastic linear elasticity equations*, Mathematical Models and Methods in Applied Sciences **24** (2014), no. 3, 513–552.

Department of Mathematics, Indian Institute of Technology Roorkee (IITR), India
E-mail address: `arbaz@ma.iitr.ac.in`

School of Mathematics, University of Birmingham, UK
E-mail address: `A.Bespalov@bham.ac.uk`

School of Mathematics, University of Manchester, UK
E-mail address: `c.powell@manchester.ac.uk`

School of Mathematics, University of Manchester, UK
E-mail address: `d.silvester@manchester.ac.uk`